Effects of ocean circulation on the eutrophication of a Mediterranean gulf with river inlets: The Northern Thermaikos Gulf

Yannis Androulidakis [a,*], Vassilis Kolovoyiannis [b], Christos Makris [a], Yannis Krestenitis [a], Vasilis Baltikas [a], Natassa Stefanidou [d], Andromachi Chatziantoniou [c], Konstantinos Topouzelis [c], Maria Moustaka-Gouni [d]

[a] Laboratory of Maritime Engineering and Maritime Works, School of Civil Engineering, Aristotle University of Thessaloniki, Greece
[b] Laboratory of Physical and Chemical Oceanography, Department of Marine Sciences, University of the Aegean, Greece
[c] Laboratory of Environmental Quality and Geospatial Applications, Department of Marine Sciences, University of the Aegean, Greece
[d] Laboratory of Botany, School of Biology, Aristotle University of Thessaloniki, Greece

ARTICLE INFO

ABSTRACT

Thermaikos Gulf is a typical, river-fed, microtidal, semi-enclosed, coastal inlet of the east-central Mediterranean Sea. It is an important coastal ecosystem susceptible to several anthropogenic pressures, strong river discharges and variable meteorological and ocean (met-ocean) conditions. One of the most significant environmental problems of the region is the occasional formation of extended eutrophication phenomena (red tides, mucilaginous aggregates), especially over the Northern Thermaikos Gulf (NTG). Herein, we investigate the contribution of hydrodynamic processes on the formation of such events, under the effects of different meteorological and river discharge conditions during the annual cycle. We conducted field observations (physical-chemical measurements), microscopy analysis of phytoplankton samples, satellite ocean color image analysis, and implemented high-resolution numerical hydrodynamic simulations with updated river discharge outflows to detect eutrophication events and correlate them with the prevailing physical processes and ocean circulation patterns. The eutrophication events were mainly associated with the dominance of southerly winds, which affect the ocean circulation over the NTG in three ways: i) they confine the surface waters in the northern parts of the NTG separating the waters masses between the northern and southern regions, ii) they contribute on the northward spreading of nutrient-rich brackish waters towards the northern parts of the Gulf, and iii) they impose an anticyclonic circulation, especially in the inner- and central-Gulf weakening its renewal process. Northerly winds contribute on the renewal of the Gulf imposing a two-layer flow, especially along the eastern coasts. The seasonal observational campaigns of the 2017–2018 period captured three eutrophication events (June–July 2017, December 2017, and May 2018) and two renewal periods (late-July 2017 and October 2017) that were favoured by the two aforementioned types of met-ocean synergy. New insight is provided on the mesoscale ocean circulation and sub-mesoscale local effects on eutrophication events in a typical microtidal coastal system of the east-central Mediterranean, where freshwater discharges by a multi-river inlet.

1. Introduction

The Northern Thermaikos Gulf (NTG), which includes the Thessaloniki Bay, is a typical Euro-Mediterranean microtidal aquatic environment located at the northwestern Aegean Sea. It is connected to the southern Thermaikos Gulf and furthermore to the Aegean Sea through its southern boundary (Fig. 1a). The main characteristics of the study region are the dense urban infrastructure along the northern part of the coastline (mainly the city of Thessaloniki; second largest in Greece), the high traffic load of commercial maritime transport in the port of Thessaloniki, the aquaculture and fishing activities in coastal waters and the open sea, the touristic activities mainly along the eastern parts of the coastal zone, the heavy industrial operations over the western region of the NTG, the discharges of nutrient-rich waters by rivers (both national and international) and drainage networks, the agricultural activities in the coastal plain of the western mainland of the NTG, and the presence

of environmentally protected areas (river deltas). Therefore, the NTG is a recipient of various pollution pressures due to several urban, agricultural, and industrial diffuse and point sources that release both treated and untreated wastewater. The investigation of the quality of the NTG is of both local and broader interest due to the large number of habitants (>1,500,000), the various human activities, and the protected areas at the deltas of transboundary rivers located along the coastal zone.

The mesoscale hydrography of the Gulf and the main sub-mesoscale circulation processes are mostly determined by the seasonal cycles of the river discharges along the western coast and the variations of the atmospheric conditions (thermal and wind) in tandem with the water mass exchanges with the open sea (Krestenitis et al., 2012). The hydrodynamic circulation of the NTG is characterized by two seasonal patterns, one during the winter and the other during summer (Hyder et al., 2002; Krestenitis et al., 2012). The intrusion of the denser Aegean Sea Waters (ASW) usually takes place through the deeper layers along the eastern coasts of the Gulf while the water masses of the Gulf exit towards the open sea through the surface layers (Balopoulos and Friligos, 1993; Krestenitis et al., 2012). Intrusion of lighter open sea waters over the surface waters may also take place along the eastern coasts of the NTG, usually induced by the Black Sea Waters signal (Androulidakis and Kourafalou, 2011). The NTG is a major source of brackish waters,

participating to the general cyclonic circulation of the North Aegean along the west coasts of Thermaikos and towards the South (Kourafalou and Barbopoulos, 2003; Kourafalou and Tsiaras, 2007; Androulidakis et al., 2012). The NTG also appears amongst the regions of dense water formation in the Eastern Mediterranean Sea, i.e., a process taking place mainly under surface water cooling by northerly gales (Estournel et al., 2005; Zervakis et al., 2005; Krestenitis et al., 2012).

The major lateral freshwater input of NTG is consisted by the four rivers (Gallikos, Axios, Loudias, and Aliakmonas; Fig. 1a) together with a large complex system of drainage canals and ditches, mainly located at the western coast (Vokou et al., 2018). The most important discharges are associated to the Aliakmonas and Axios rivers (Fig. 1b), which form multi-channel deltaic systems (Karageorgis et al., 2000, 2005; Krestenitis et al., 2012). Fig. 1b presents recent available discharge time series for both the Aliakmonas and Axios braided fluvial systems (for more information see Section 2.3). The generally strongest river outflow of Axios is the most polluted in terms of nutrient concentrations (Skoulikidis et al., 1993; Karageorgis et al., 2005; Nikolaidis et al., 2006; Tsiaras et al., 2014) and is characterized by a clear seasonal signal with high rates in spring and low rates in late summer. For Aliakmonas river, the existence of four dams along its watercourse determines the temporal variability of the outflow with a weaker seasonal signal (Krestenitis
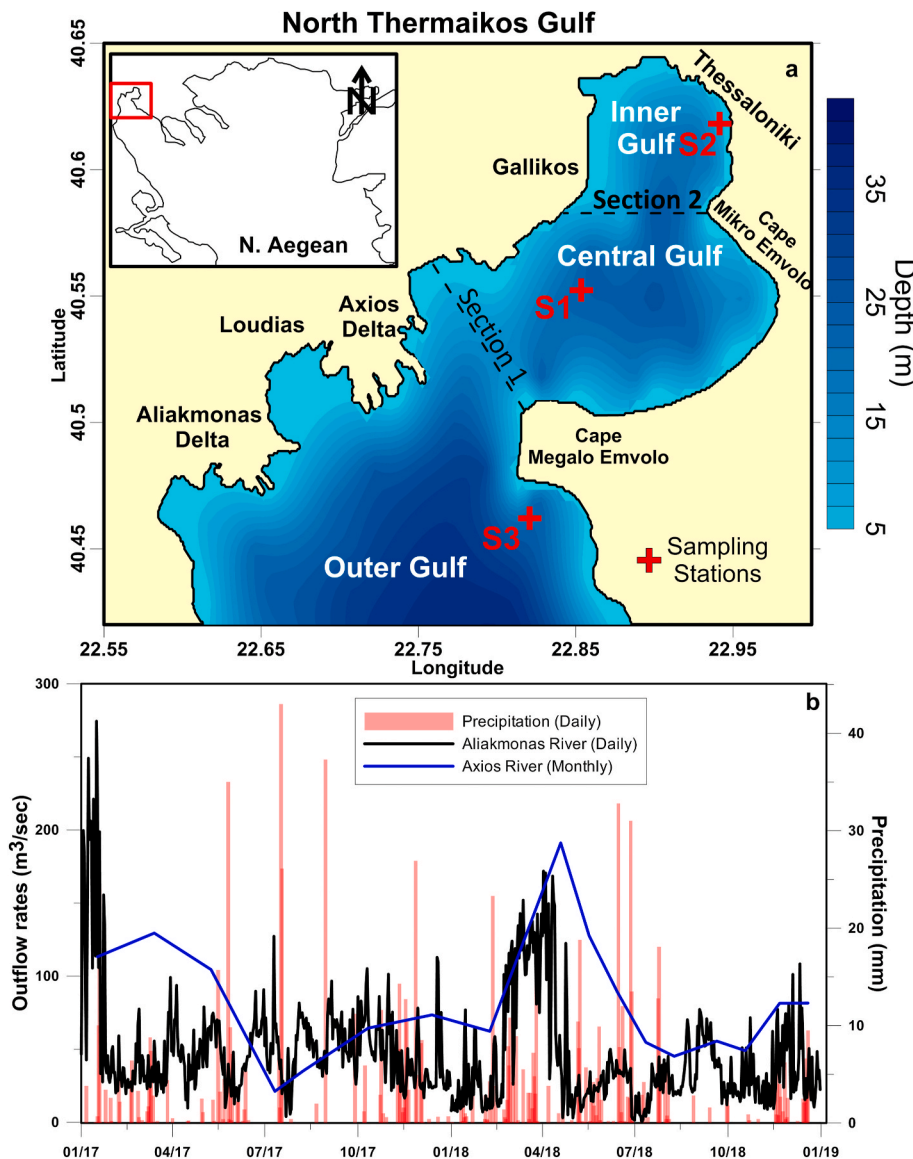
Fig. 1. (a) Bathymetry of the Northern Thermaikos Gulf, located in the Northwestern Aegean Sea (insert in the upper left). The major topographic features (inner-, central- and outer-Gulf, Cape Megalo Emvolo, Cape Mikro Emvolo, city of Thessaloniki, Gallikos, Axios, Loudias and Aliakmonas rivers) of the Gulf are shown. The location of three sampling stations are also marked with red crosses. Dashed black lines indicate the borders between the three sub-regions (Sections 1 and 2). (b) Timeseries of Aliakmonas (black line; daily values) and Axios (blue line) discharge rates for 2017–2018. The pink bars represent the daily precipitation rates, measured by AUTh's meteorological station (data provided courtesy of DMC; https://meteo.geo.auth.gr/el/meteo-obs).

et al., 2012; Skoulikaris and Krestenitis, 2020). The formation of the river plumes that control the initial distribution of the riverine loads is influenced by the proximity of the Thermaikos east and west coasts (Kourafalou et al., 2004), affecting the biochemical properties of the rather shallow NTG (Poulos et al., 2000; Karageorgis et al., 2005).

The hydrography of the region, the major circulation patterns, and several physical processes (e.g., coastal upwelling, dense water formation, renewal, river plume dynamics, vertical mixing) play a significant role on the variability of the ecological and biogeochemical characteristics, the pollutants transport, and furthermore the water quality of the Gulf.

The main motivation of this study is to investigate the influence of the predominant circulation patterns on the appearance of eutrophication events based on an integration of satellite, *in situ* and modeling data. Eutrophication events are very common in Thermaikos Gulf, especially pronounced over the northern region, and have recently raised great concern among the public, municipal, and regional authorities, and the scientific community. Nikolaidis et al. (2005) report that the NTG red tide incidents were the first documented marine toxic outbreaks in Greece, which resulted in economic losses of about 5×10^6 € for the Greek shellfish industry. These events are strongly related to the inflow of nutrients and other organic pollutants from the mainland into coastal waters, especially through the area's river system (Gotsis-Skretas and Friligos, 1990; Balopoulos and Friligos, 1993; Pagou et al., 2000; Karageorgis et al., 2005; Nikolaidis et al., 2006; Petala et al., 2018; Genitsaris et al., 2019).

Although marine eutrophication has received much attention due to its ramifications on coastal ecosystems, comparatively few studies focus on the quantitative relationship between water circulation dynamics and trophic conditions in enclosed ecosystems. Most of the studies worldwide, focused on the effects of specific physical properties and processes, such as water temperature, seasonal stratification, coastal upwelling, and inflows of freshwater on eutrophication phenomena at coastal waters (e.g., Sur et al., 1994; Rabalais et al., 2009; Skogen et al., 2014; Cabral et al., 2020). The eutrophication state and its relation to physical and biological interactions were studied by Lee et al. (2006) for the Hong Kong coastal waters, an area with high nutrient loads; it is shown than met-ocean conditions (e.g., wind and tidal mixing) control the formation of blooms. Sur et al. (1994) showed that the advection of materials over the Black Sea continental shelf created along the boundary current, are important for the spreading of productivity and the evolution of eutrophication processes. Ferrante et al. (2013) reviewed the formation of Harmful Algal Blooms (HABs) in the Mediterranean and related it to typical sub-mesoscale phenomena of localized circulation dynamics constrained in coastal areas, such as bays, lagoons, ports, beaches, and estuaries. They reported that coastal blooms of the Mediterranean are an emerging problem related to nutrient enrichment of coastal waters mostly by river inlets or coastal watersheds. However, they inferred that the influence of sub-mesoscale coastal circulation on HABs in such environments has not been thoroughly investigated yet. Lévy et al. (2018), in their review, discussed the formation of sub-mesoscale patchiness and the ways it could drive impacts on phytoplankton growth rates, e.g., strong vertical currents and mixing processes bringing nutrients into the euphotic zone, causing rapid, local increases of phytoplankton growth rates. Advection processes (stirring and mixing by ocean currents) of planktonic features are therefore investigated, yet mostly focusing on the vertical basin-scale ocean circulation. Based on the comprehensive recent review of Zohdi and Abbaspour (2019), only very few studies to date have analyzed to what extent the ocean dynamics may affect the eutrophication states (HABs formation and red tides) or the water renewal of semi-enclosed gulfs with significant river discharges, such as the NTG. Herein, we focus on the impact of the fine-scale circulation dynamics on renewal processes of a coastal semi-enclosed region that is influenced by strong river loads.

The main three questions that arise are:

1) Which ocean circulation patterns may contribute to the enhancement of eutrophication in typical, microtidal, semi-enclosed gulfs of the Mediterranean?
2) What is the relation between the meteorological conditions and the ocean dynamics during eutrophication or renewal periods?
3) Are the renewal processes important for the reduction of eutrophication in our case study?

To address these questions, we initially divided the NTG into three sub-regions on the basis of their geomorphological and functional characteristics: 1) the inner-Gulf, which is a shallow and semi-enclosed bay at the northern part of the Gulf between the seafront of Thessaloniki city and the Cape Mikro Emvolo, 2) the central-Gulf, which is located between the inner-Gulf and the Cape Megalo Emvolo, and 3) the outer-Gulf, south of the Cape Megalo Emvolo, including the two large river deltas of Axios and Aliakmonas (Fig. 1a). We then analyzed *in situ* seasonal measurements, collected at the three NTG sub-regions (Fig. 1a) from summer of 2017 to spring of 2018 in tandem with satellite ocean color images and numerical modeling of the 3-D circulation (Section 2). We aimed to detect events characterized by either eutrophication symptoms (phytoplankton blooms, "red tides", "dirty sea mucilaginous aggregates") or strong renewal processes ("clear waters") (Section 3) and to discuss the prevailing meteorological and oceanic conditions during these periods (Section 4).

2. Methods and data

2.1. In situ observations

The seasonal *in situ* measurements refer to the physical (temperature and salinity) and chemical (chlorophyll-a: chl-a) parameters, whereas water samples for phytoplankton microscopy analysis were also collected in the water column of three sampling stations, located at the inner- (Station S2), central- (Stations S1), and outer- (Station S3) Gulf (Fig. 1a). The observational period covered an annual cycle, including four seasons from summer 2017 to spring 2018. Information of the

Table 1
Characteristics of the three sampling stations (coordinates, depth, region) and list of observational datasets used in the study. The seasons and areas with not available data are noted.

Sampling Station	Station S2	Station S1	Station S3
Station Longitude (°E)	40.618	40.552	40.462
Station Latitude (°N)	22.941	22.853	22.820
Depth (m)	13	25	30
Region	Inner-Gulf	Central-Gulf	Outer-Gulf
In situ temperature	05/07/17 20/07/17 10/10/17 11/12/17 05/18	20/07/17 10/10/17 11/12/17 17/05/18	05/07/17 20/07/17 10/10/17 11/12/17 05/18
In situ Salinity	05/07/17 20/07/17 10/10/17 11/12/17 05/18	20/07/17 10/10/17 11/12/17 17/05/18	05/07/17 20/07/17 10/10/17 11/12/17 05/18
In situ Chl-a	20/07/17 10/10/17 11/12/17 17/05/18	20/07/17 10/10/17 11/12/17 17/05/18	20/07/17 10/10/17 11/12/17 17/05/18
Phytoplankton Biomass	20/07/17 10/10/17 11/12/17 17/05/18	20/07/17 10/10/17 11/12/17 17/05/18	20/07/17 10/10/17 11/12/17 17/05/18
Current velocities	–	14/11/19	14/11/19
Meteorological data (wind and precipitation)	All Seasons (3-hourly step for 2017 and daily step for 2018)		
Satellite Sea Surface Temperature	All regions & all seasons		
Satellite Ocean Color chl-a	All regions & all available images		

sampling campaigns are presented in Table 1. The physical oceanographic parameters were recorded at the entire water column with the use of a Conductivity-Temperature-Depth (SBE 19plus V2 SeaCAT Profiler CTD by Sea-Bird Scientific), equipped with a Fluorescence sensor (Wet Labs ECP-AFL/FL; mg/m^3). The collected data provide information about the depth, temperature, salinity (derived from conductivity) and chl-a concentrations distribution from the surface to the bottom of the sea. All raw data were processed with SBE Data Processing (Sea-Bird Scientific, 2017) and fluorescence was converted to chl-a concentration.

During CTD recordings, *in situ* processing of the physical parameters enabled the preliminary determination of the water column stratification (Androulidakis et al., 2018). Then, seawater samples were collected from three levels of the water column (surface, pycnocline, and bottom) with a standard Model 1010 Niskin Water Sampler (1.7 L), in order to investigate the recorded variations of biological parameters over the water column depth (Petala et al., 2018). Water subsamples (fresh, 250 mL) were placed in a portable refrigerator and preserved subsamples were immediately fixed with Lugol's iodine. Fresh and preserved water samples were examined under a light inverted microscope (Nikon SE, 2000), and species were identified using appropriate taxonomic keys. Unicellular planktonic organism counts were performed using the sedimentation method of Utermöhl (1958). Briefly, at least 400 plankton individuals were counted in each sample in sedimentation chambers of 3, 10, 25 or 50 mL, depending on the total abundance in each sample. In order to estimate the fresh weight of phytoplankton, the dimensions of 30 individuals (cells, or colonies) of each dominant species (comprising of ≥10% of the total phytoplankton in terms of abundance and biomass) were measured using the relevant tools of a digital microscope camera (Nikon DS-L1). Mean cell, or colony volume estimates were calculated using appropriate geometric formulae according to Hillebrand et al. (1999).

The vertical distribution of horizontal currents was also derived at two stations (Stations S1 and S3) on 14/11/19 with the use of an Acoustic Doppler Current Profiler (ADCP), namely the Workhorse Sentinel ADCP by TELEDYNE MARINE. The instrument was moored at the bottom of each station for 20 min and collected horizontal velocities at the entire water column. The measured vertical distribution of current velocities provided information about the circulation of different water masses and the renewal of the inner-NTG.

Meteorological data for the study period, including precipitation and wind speed and direction, were obtained from the Aristotle University of Thessaloniki (AUTh) station provided by the Department of Meteorology and Climatology (DMC). The wind data were used to examine the prevailing wind conditions during the observational campaigns from summer 2017 to spring 2018. Additionally, the recorded precipitation values were used to investigate the contribution of rainwater to the physical variables' distribution and to characterize the surficial buoyant discharges.

2.2. Satellite data

Two types of satellite data were used during the annual cycle, one for ocean color and one for sea surface temperature. The first one derives the chl-a concentrations over the entire study region using ocean color information. All the collected raw satellite images refer to Sentinel-2 and Sentinel-3 datasets, derived from EU's Earth Observation Programme platform, Copernicus (https://scihub.copernicus.eu/). The Sentinel-2 satellite has a spatial resolution of 10 m in visible (RGB) and NIR bands and a revisit time of 5 days. For Sentinel-2 satellite, the Level-1C product was used. After pre-processing (atmospheric correction, land mask and cloud mask), the Case-2 Regional Coast Color (C2RCC; Brockmann et al., 2017) algorithm was applied to estimate chl-a concentrations. C2RCC uses a large database of radiative transfer simulations, inverted by neural networks, for the derivation of the chl-a concentration product. In addition, data were collected from Sentinel-3 satellite i.e., the Ocean and Land Color Imager (OLCI) Instrument. OLCI uses optical bands to retrieve ocean images with 300 m spatial resolution and daily revisit. Chlorophyll concentrations from Sentinel-3/OCLI is a standard Level-2 product, derived from the OC4Me Chlorophyll algorithm (Morel et al., 2007). We used both satellites (Sentinel-2 and Sentinel-3) to increase the temporal resolution (a five-days step with 10 m resolution and a daily step with 300 m resolution). We produced horizontal maps of chl-a concentrations during all observational campaigns (Table 1) and computed the mean concentrations from all available images, averaged over the study sub-regions, to detect potential blooms, eutrophication events and different types of water masses (e.g., river plumes, ASW, clear waters, etc.).

The second type of satellite data is the Sea Surface Temperature (SST) set by JPL OUROCEAN product, derived from the Group for High Resolution SST project (GHRSST; ftp://ftp.nodc.noaa.gov/pub/data.nodc/ghrsst/L4/GLOB/JPL_OUROCEAN/G1SST). We used the Level 4 SST data produced as a retrospective dataset at the NASA Jet Propulsion Laboratory Physical Oceanography Distributed Active Archive Center (DAAC). The SST was derived using wavelets as basis functions within an optimal interpolation approach on a global 0.011° grid. The SST fields were used to detect the different types of water masses during each observational campaign, in tandem with model results (see Section 2.3), *in situ* measurements, and ocean color maps.

2.3. Numerical simulations

The numerical simulations were implemented with the FLOW module of the Delft3D (Delft3D-FLOW) modeling system (https://oss.deltares.nl/web/delft3d) in a 3-dimensional (3-D), sigma-layer configuration for the investigation of the NTG hydrodynamic circulation (Delft3D-Thermaikos model; Krestenitis et al., 2020). The model solves numerically the 3-D non-linear shallow water equations, derived from the 3-D Navier-Stokes equations for incompressible, free-surface flow. Apart from the horizontal equations of motion, the system of model equations consists of the continuity equation and the transport equations for conservative constituents (Deltares, 2018). Real-world applications' validation and model description of Delft3D-FLOW can be found in Lesser et al. (2004) and Gerritsen et al. (2007).

In this study, the model domain of Delft3D-Thermaikos covers the broader Thermaikos Gulf (22.55–23.374°E and 39.96–40.643°N) and is defined by a 110 × 126 curvilinear grid, with a resolution step varying from about 750 m offshore near the open boundary (North Aegean Sea) to less than 350 m in the inner-Gulf. In the vertical, 15 sigma layers were used to discretize the water column. The sigma-layers configuration allows model coordinates to follow the bottom morphology and is suitable for Mediterranean coastal regions with shallow and complex topography (Zavatarelli and Mellor, 1995) such as the NTG. The open southern boundary of the model (boundary interconnection between Thermaikos Gulf and North Aegean Sea) was forced by timeseries of temperature and salinity profiles, and sea surface height provided by the Mediterranean Forecasting System model (Clementi et al., 2019; http://medforecast.bo.ingv.it/) embedded into CMEMS Mediterranean Sea Physical Reanalysis dataset (Simoncelli et al., 2019). The meteorological forcing was derived from the met-ocean weather forecast operational system developed and operated in the context of the WaveForUs project (Krestenitis et al., 2014, 2015; http://wave4us.web.auth.gr). Meteorological simulations were conducted by AUTh's DMC, based on the Weather Research and Forecasting model with the Advanced Research dynamic solver (WRF-METEO-AUTh; Wang et al., 2010; Pytharoulis et al., 2014). The produced 3-hourly atmospheric datasets (wind velocities, sea level pressure, air temperature, relative humidity, cloudiness, and precipitation fields) cover the Central Macedonia region with a spatial resolution of approximately 1600 m.

The freshwater inflows from the four main rivers discharging into the basin (Axios, Aliakmonas, Loudias, Gallikos; Fig. 1a), used as lateral input for the Delft3D-Thermaikos simulations, were parameterized as follows:

- For Axios river, flow rate measurements (seven values for 2017 and ten values for 2018; Fig. 1b) provided by the Soil and Water Resources Institute (https://www.swri.gr/) were used to reconstruct daily discharge rates with the help of a piecewise cubic Hermite interpolating polynomial function fitted through these measurements.
- For Aliakmonas river, whose outflow is strongly influenced by dam operation, the methodology proposed by Skoulikaris and Krestenitis (2020) was used to provide daily discharge rates (Fig. 1b). This approach relies on the use of custom-made web scrapping tools to access dams' hourly outflows in combination with water demand data, in order to investigate the water balance, as modified by human intervention, in areas located downstream of the dams. The modeled net water discharges of downstream Aliakmonas river were proved to be accurate on a daily timescale by Skoulikaris and Krestenitis (2020).

- Loudias and Gallikos flow rates were parameterized as fractions of Axios flow rate, 20% and 2% respectively, as suggested in recent literature (Alexandridis et al., 2015; Veranis et al., 2011; Mattas et al., 2014). Loudias river provides a minor input, which is only significant during summer, when it exhibits maximal outflow as the result of collected irrigation drainage (Smardon, 2009). Gallikos river is mainly arid and contributes to the freshwater supply only in cases of very intense rainfall, draining the neighbouring Axios river overflows.

3. Results

We use *in situ* and satellite ocean color images to detect eutrophication and renewal (clear waters) events during the seasonal observational campaigns. The categorization of the events is based on the *in situ* chl-a and phytoplankton biomass concentrations collected in the three
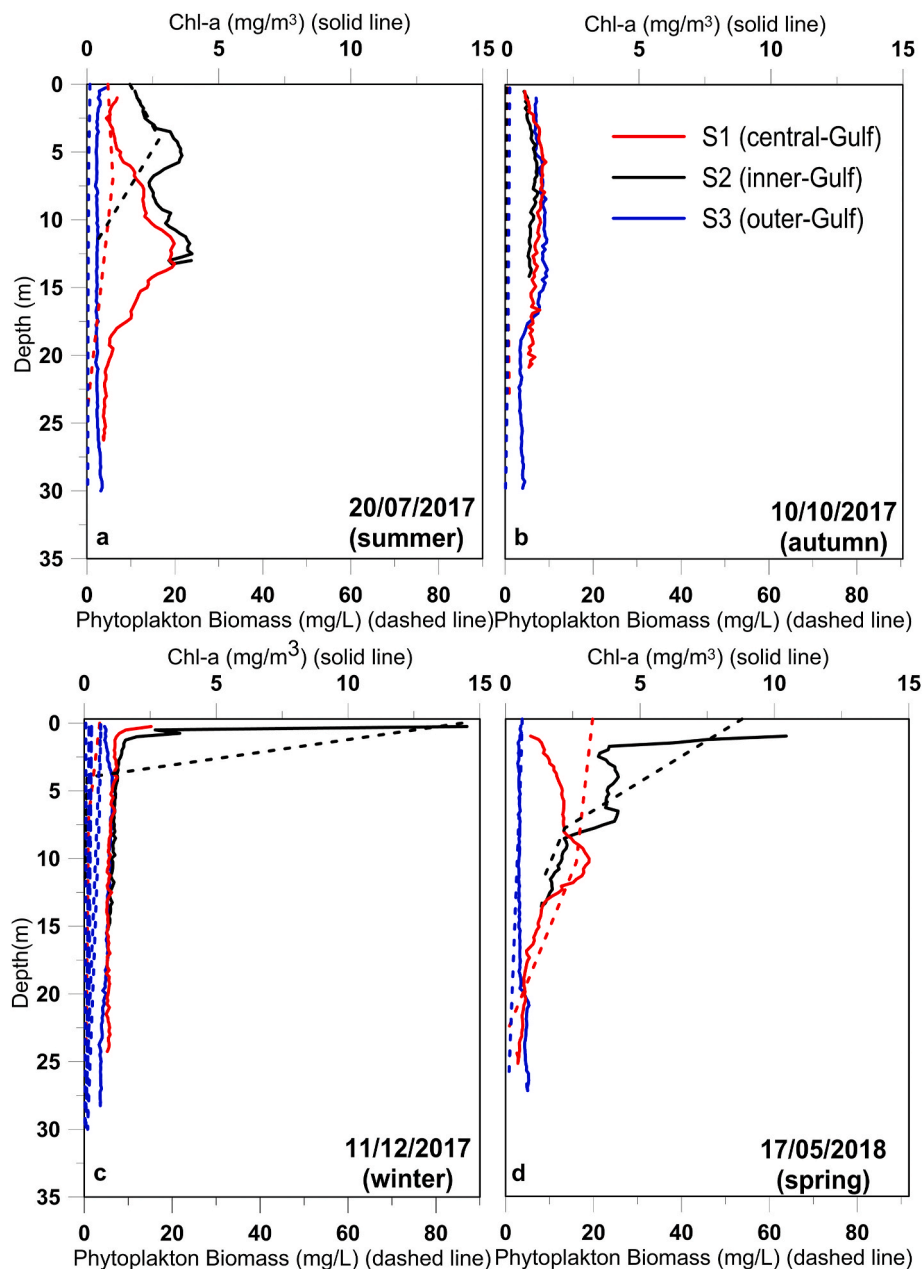
Fig. 2. Seasonal vertical profiles of chl-a measured by SBE 19plus CTD (mg/m³; solid lines) and phytoplankton biomass (mg/L; dashed lines) at S1 (red line), S2 (black line), S3 (blue line) stations on (a) 20/07/17, (b) 10/10/17, (c) 11/12/17, and (d) 17/05/18. Measurements and samples were not collected only on 05/07/17 (Table 1).

sampling stations in tandem with the broader coverage of chl-a levels provided by the satellite. High and low concentrations are associated to eutrophication and renewal events, respectively.

3.1. Detection of eutrophication events by observational campaigns

The distribution of chl-a in the water column and the phytoplankton biomass concentration at specific depths for each campaign and sampling station are presented in Fig. 2. The chl-a water column distribution derived with the CTD broadly agrees with the distribution of the phytoplankton biomass derived from processing of collected water samples in three depth levels (surface, pycnocline, near-bottom). The peak values and the distributions between the two variables qualitatively agree in all cases despite the very low chlorophyll content of phytoplankton biomass reflecting the physiological state of dominant diatoms and the mixotrophy of other phytoplankters on their chl-a content (Genitsaris et al., 2019). The respective horizontal distribution of chl-a, derived from the satellite ocean color images, is presented in Fig. 3. Although patches of high chl-a were mainly detected in the proximity of the river deltas and usually along the respective coasts in almost all cases due to the high nutrient load, high concentrations were also detected in the broader NTG. The highest near-surface chl-a values among the three stations were detected over the inner-Gulf (Station S2) in early-December 2017 ($\sim$15 mg/m^3; Fig. 2c) and in May 2018 ($\sim$10 mg/m^3; Fig. 2d). The phytoplankton biomass also revealed the highest values (85 and 55 mg/L) during these two dates, while smaller, but relatively high concentrations were detected in July 2017 (20 mg/L; Fig. 2a) in agreement with the chl-a concentrations (2–4 mg/m^3). In all seasons, Station S3 (outer-Gulf) revealed very low and homogenous vertical distribution of chl-a ($\sim$1 mg/m^3) and phytoplankton biomass ($<$5 mg/L) indicating lower primary production of nano- and micro-phytoplankton over this area, located closer to the open sea boundary (influence of clear waters). The lowest chl-a and phytoplankton values at all sampling areas were observed on October 10, 2017 with values around 1 mg/m^3 and less than 1 mg/L throughout the water column, respectively (Fig. 2b), indicating lower primary production over the entire NTG. The physical characteristics and circulation processes, associated to the high and low eutrophication levels presented above, are discussed in Sections 3.3 and 4.

High chl-a concentrations were detected by the satellite ocean-color sensor in early-July 2017 (Fig. 3a), when in situ chl-a measurements and phytoplankton samples are not available (Table 1). Different surface distribution of satellite-derived chl-a was observed in the ocean color satellite images between the two campaigns of summer 2017 (July 5 and 20). However, the satellite-derived chl-a was still relatively high in the inner part of the NTG on 23 July (Fig. 3b) in agreement with the in situ measurements at Station S2 (Fig. 2a). The satellite-derived chl-a concentrations ranged around lower values at the end of July in the central- and outer-Gulf (Fig. 3b) in agreement with the in situ measurements on July 20 (Fig. 2a). The eutrophication event in late-June and early-July was related to an extensive phytoplankton bloom in spring-early summer 2017 (Fig. 4a) and Noctiluca red tides that contributed to a dirty sea phenomenon of mucilaginous aggregates (Genitsaris et al., 2019). Extensive spreading of brackish waters over several parts of the Gulf was detected by the Sentinel RGB image on July 3 (Fig. 4c). The satellite ocean color images confirm the high chl-a and phytoplankton biomass concentrations in December 2017 (Fig. 3e) and May 2018 (Fig. 3h) as also identified by the in situ measurements (Fig. 2c and d). The December 2017 red tide event was also discussed by Genitsaris et al. (2019), which was related to the autotrophic ciliate species Mesodinium rubrum (Fig. 4b). Based on the ocean color images, the chl-a concentrations were significantly high south of the Axios Delta on December 5 (Fig. 3d) but were also increased in the inner-Gulf a few days later, on December 10 (Fig. 3e), in agreement with the field observations. The eutrophication event was almost absent on 20 December (Fig. 3f); this variation was strongly affected by the prevailing met-ocean conditions (see Section

4.1). Winter and spring of 2018 was characterized by very strong river discharges by both Axios ($>$160 m^3/s) and Aliakmonas ($>$150 m^3/s) rivers (Fig. 1b), supplying the NTG with high quantities of nutrients. Genitsaris et al. (2019) detected phytoplankton blooms in February 2018 that could be associated with the nitrogen pollution of intense agricultural activity, draining waters towards the sea through the river outflows. The river discharge effects on the chl-a levels of the coastal areas, especially along the western coast of the NTG, are identified on May 14 (Fig. 3g), a few days before the observational campaign on May 17. The spreading of brackish surface waters over the NTG was also confirmed by RGB images collected by the Sentinel satellite on both December 11, 2017 (Figs. 4e) and May 17, 2018 (Fig. 4f). Most of the phytoplankton species were found common in the three stations (not shown). Station S1 (central-Gulf), which is located closer to the river deltas, shows the richest phytoplankton species pool (71 species). Phytoplankton communities in S2 and S3 were an almost strict subset of the phytoplankton species pool inhabiting S1 with only 2 and 3 different species, respectively. Phytoplankton species pool includes fast-growing nutrient opportunists (e.g., flagellates and diatoms) forming blooms, supporting the contribution of the nutrient-rich river waters on the eutrophication formation of all NTG's regions. The river effects on eutrophication events under the prevailing ocean circulation conditions are discussed in Sections 3.2 and 4.1.

Generally, both in situ (Station S3) and satellite data support the lower eutrophication state over the southeastern part of the NTG, while the higher chl-a concentration values usually appeared in the inner-Gulf and especially along the western coasts, where the river deltas are located. The year of 2017 was unique, with two very intense eutrophication events (late-June to early-July 2017 and December 2017) and two periods characterized by clear waters (late-July 2017; October 2017; Figs. 3 and 4) over the entire NTG and are discussed with respect to the prevailing circulation features in Sections 4.1 and 4.2, respectively.

3.2. Water column distribution of physical characteristics

The vertical profiles of temperature (Fig. 5) and salinity (Fig. 6) were derived by in situ CTD measurements during 5 campaigns covering periods of extended eutrophication events (summer, winter, and spring) and a period without eutrophication (clear waters; summer and autumn). The physical properties are presented in tandem with the respective satellite-derived SST maps, overlaid with the concurrently prevailing wind conditions (Fig. 7) in order to identify the different water masses during each campaign.

During the eutrophication event in late-June and early-July 2017, cold ($<$15 °C; Fig. 5a) and saline ($>$38; Fig. 6a) waters were detected near the bottom of the outer-Gulf (Station S3), indicating water masses that originated from the North Aegean (ASW). Very strong thermocline and halocline were detected at a depth of around 12 m in the outer-Gulf, where the surface temperature and salinity ranged around 26 °C and 36, respectively. On the contrary, the upper layers of the inner-Gulf were occupied by a different water mass with lower surface temperature ($\sim$24 °C; Fig. 5a) and salinity ($\sim$35; Fig. 6a). The different surface water masses between the northern and southern areas of the NTG are also apparent in the satellite SST images (Fig. 7a); colder water masses occupied the entire inner-Gulf, while the central and southern regions were approximately 2 °C warmer in agreement with the in situ measurements. The deeper waters of the inner-Gulf are characterized by relatively lower temperature (21 °C; Fig. 5a) and significantly high salinity values ($>$38; Fig. 6a). However, these waters are separated from the near-surface layers which are covered by lower salinity waters originated from the rivers, located along the western coast of Gulf. The Aliakmonas river discharges ranged around 100 m^3/s, while precipitation rates were zero during this eutrophication event (late-June and early-July; Fig. 1b). It is concluded that the upper inner-Gulf is covered by a distinct water mass, different than the deeper and outer-Gulf
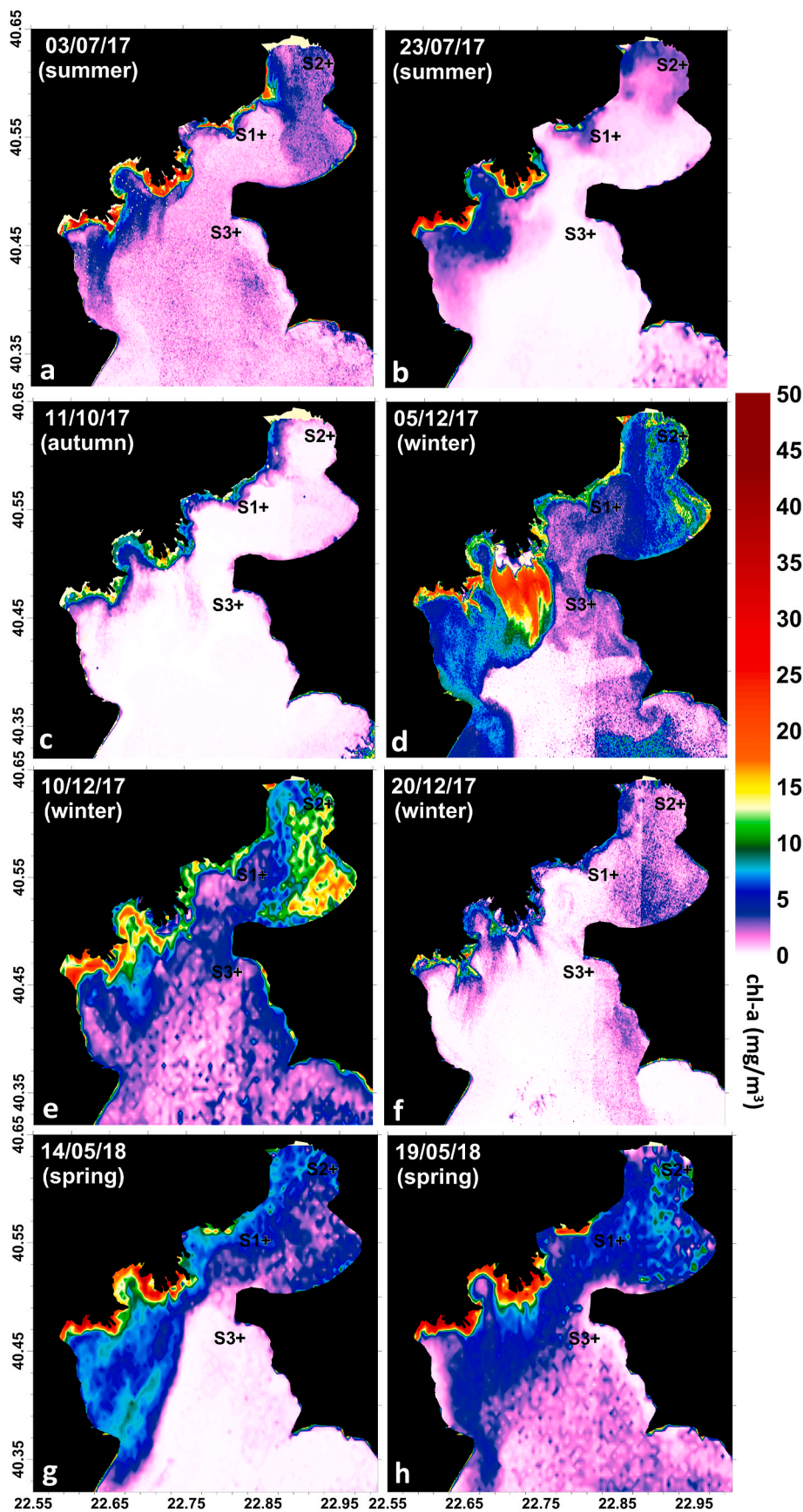
Fig. 3. Horizontal distribution maps of chl-a concentrations (mg/m^3), derived from the available Sentinel-2 and Sentinel-3 satellite on (a) 03/07/17, (b) 23/07/17, (c) 11/10/17, (d) 05/12/17, (e) 10/12/17, (f) 20/12/17, (g) 14/05/18, and (h) 19/05/18. The locations of the Stations S1, S2 and S3 are marked with crosses.
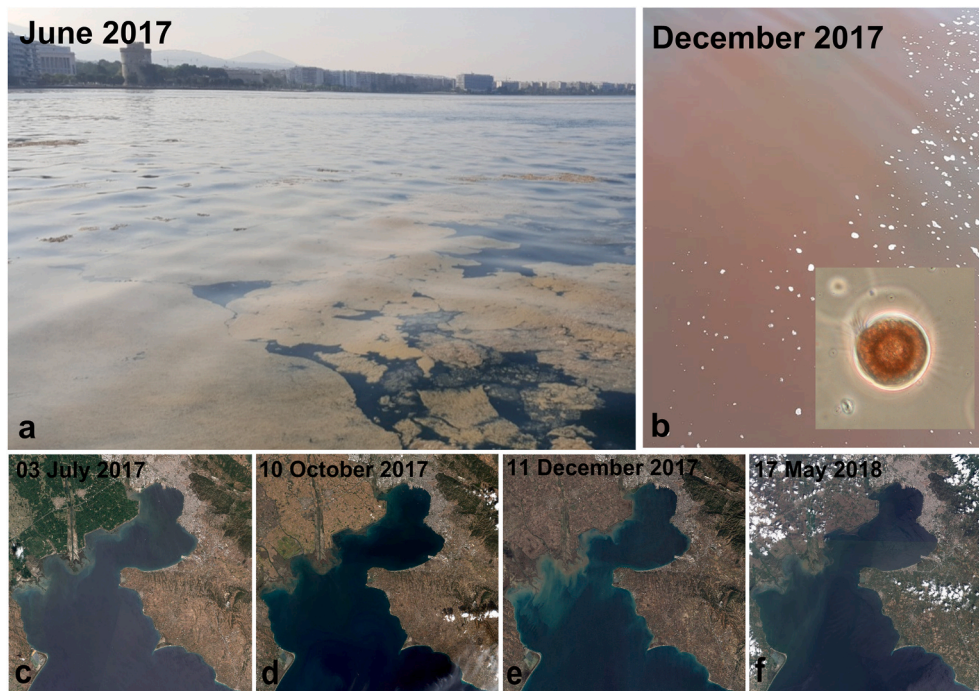
Fig. 4. Eutrophication events, captured in the inner-Gulf (a) in late-June 2017 (dirty sea phenomenon; Genitsaris et al., 2019) and (b) in early-December 2017 (red tide phenomenon). The microscope depiction of *Mesodinium rubrum*, responsible for the red tide event in December is presented in the insert of panel (b). Sentinel-2 satellite RGB images are shown for (c) July 03, 2017, (d) October 10, 2017, (e) December 11, 2017, and (f) May 17, 2018.

waters. As presented in Section 3.1, this water mass revealed excessive eutrophication and dystrophication (Fig. 4a) in late-June and early-July 2017 (Genitsaris et al., 2019). The arising question is whether the ocean circulation due to southerly winds that prevailed before the eutrophication event (Fig. 7a), in tandem with the strong stratification, contributed to the formation of this event over the inner-Gulf (see Section 4.1). The northerly winds that prevailed around July 4, after a long period of southerly winds (Fig. 7a), were successful in degrading the mucilaginous surface layer and disperse it as small mucilage aggregates (Genitsaris et al., 2019). The phytoplankton biomass and chl-a concentration levels were still relatively high in the inner-Gulf a few days later (July 20; Fig. 2a) when the waters masses were also characterized by low salinity levels (Fig. 6a) although the water column was warmer and more homogenous in comparison to early-July (Fig. 5a). The central- and outer-Gulf consisted of colder and more saline waters with lower chl-a and phytoplankton biomass concentrations than the inner-Gulf, indicating a more homogenous water mass between these two regions (central/outer) on July 20 after a period of northerly winds in mid-July (Fig. 7b).

A profound period of clear waters over the entire NTG was detected in early-October 2017, when persistent northerlies prevailed (Fig. 7c). The temperature (21 °C; Fig. 5b) and salinity (37; Fig. 6b) profiles support the existence of a homogenous water mass over the entire region; only the deeper layers of Station S3 were consisted of colder and more saline waters. This near-bottom layer water mass originated from the open sea and intruded towards the outer-Gulf along the eastern coast (see Section 4.2). The northerly winds kept the low salinity waters away from the northern parts of the NTG (Fig. 3c). Although Aliakmonas river discharges were relatively high in autumn (Fig. 1b), the wind-induced circulation was not able to spread the brackish waters over the entire NTG.

Different water masses between the outer-Gulf and northern parts of the NTG were also identified during the red tide event in early-December 2017 (Fig. 4b). Both inner- and central-Gulf stations revealed similar temperature (12.5 °C; Fig. 5c) and salinity (37; Fig. 6c) distribution throughout the entire water column (homogenous structure). The outer-

Gulf area (Station S3) was warmer (15.5 °C) with a slight salinity increase in the deeper layers between 15 and 22 m. The difference (~2.5 °C) between the northern and southern regions is also confirmed by the satellite SST distribution indicating the clear dominance of a distinct warmer water mass over the southeastern NTG (Fig. 7d). This region, which revealed significantly lower chl-a and phytoplankton biomass values than the inner-Gulf (Figs. 2c, 3d and 3e), was occupied by ASW that originated from the open sea but were not further advected to the central- and inner-Gulf. The meteorological conditions during the previous 20 days were characterized by both northerly and southerly winds (Fig. 7d); the southerly winds occurred during the first 5 days of December and again on December 9 after 5 days of persistent northerlies. Petala et al. (2018) showed that very high levels of Total Phosphorous (>6 μmol/L) were detected in early-December 2017 in the inner-Gulf (Station S2) while concentrations less than 1 μmol/L were detected in the outer-Gulf (Station S3). The high levels of phosphorous are usually related to the spreading of riverine waters (Fig. 4e) that are high in nutrients (Karageorgis et al., 2005) and may be advected towards the inner-Gulf under southerly winds. The occurrence of southerlies during the first 10 days of December led to the different distribution of chl-a derived by the satellite ocean color images between December 5 and 10 (Fig. 3d and e; see Section 4.1).

The eutrophication event in May 2018 was also characterized by different physical features between the outer-Gulf and the northern semi-enclosed regions of the NTG (Figs. 5d and 6d). More saline, colder, and vertically homogenous waters were observed in Station S3, while both Stations S1 and S2 revealed a similar stratified vertical structure. The satellite temperature distribution clearly confirms the colder water mass that covered the southeastern NTG while warmer waters were detected in the inner- and central-Gulf after a period of strong southerly winds (Fig. 7e). The large discharge rates of Axios and Aliakmonas rivers in spring of 2018 (Fig. 1b) supplied freshwaters in the Gulf that were still apparent over the central and especially the inner-Gulf in late-May 2018 (Fig. 6d), when high chl-a (Fig. 3g and h) and phytoplankton biomass concentrations were also detected (Fig. 2d).

The temperature, salinity, and wind measurements in tandem with
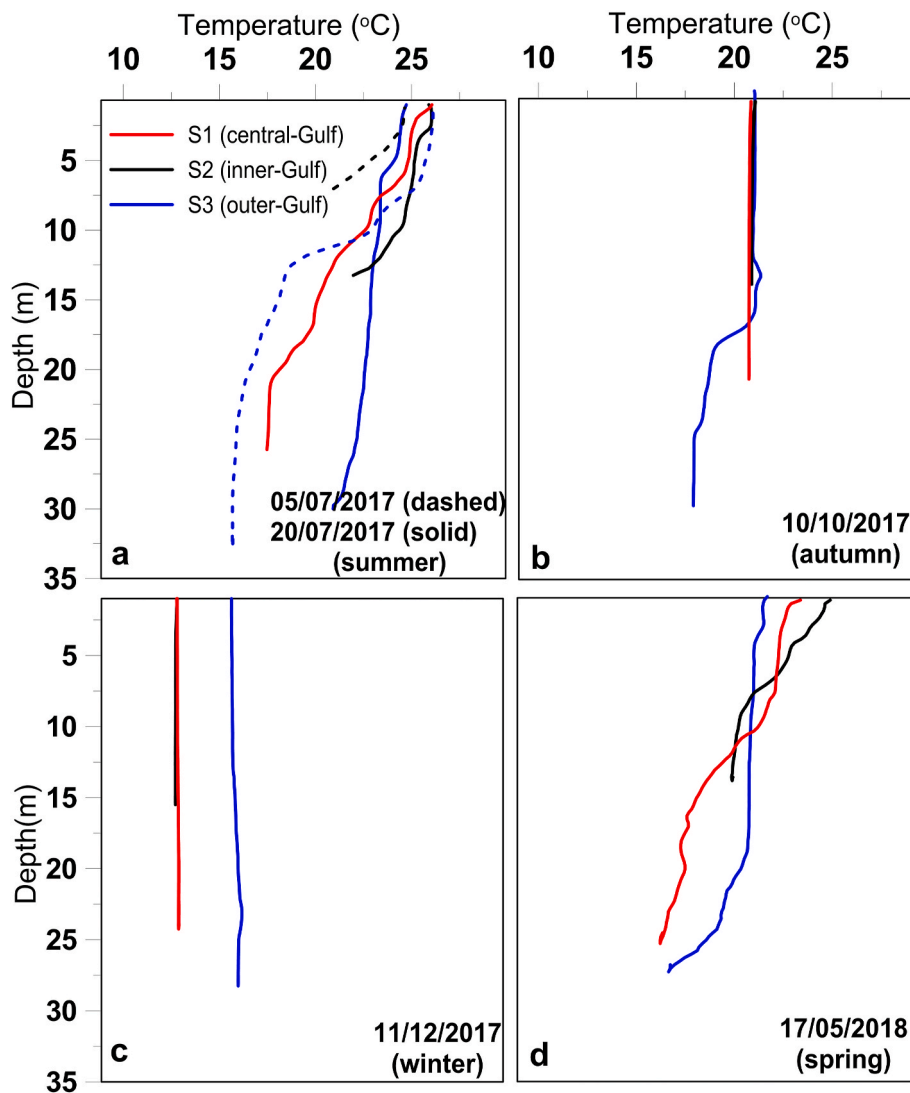
Fig. 5. Vertical profiles of seawater temperature (CTD) at S1 (red line), S2 (black line), S3 (blue line) stations on (a) 05/07/17, 20/07/17, (b) 10/10/17, (c) 11/12/17, and (d) 17/05/18. Measurements at Station S1 on 05/07/17 were not available.

the satellite SST observations revealed that the three eutrophication events were related to the southerly winds which contributed on the advection of brackish waters over the central- and inner-Gulf, separating the water masses between the outer-Gulf and the northern NTG. The prevailing mesoscale and localized circulation patterns during the formation of eutrophication events or renewal processes are further discussed in Sections 4.1 and 4.2.

3.3. Numerical simulation of ocean circulation

The Delft3D-Thermaikos model simulated the ocean circulation during a full annual cycle in 2017, covering the two major eutrophication events in late-June and early-July, and December and the two renewal events in late-July and October. The good performance of the model is discussed in Fig. 8. Salinity (Fig. 8a) and temperature (Fig. 8b) comparisons showed a very good agreement between model and observational data with high Pearson correlation coefficients ($R_{Pearson} = 0.92$ for salinity and $R_{Pearson} = 0.99$ for temperature) that are statistically significant based on the Mann-Kendall (MK) test (Mann, 1945; Kendall, 1975) for a *p*-value scoring <0.01 (i.e., at least 1% significance or 99% confidence levels). The coefficients of determination ($R^2 > 0.85$) also confirm the efficiency of the model to reproduce the values of the measured physical parameters at all areas, depths, and periods. The

RMSEs are relatively small for both variables and the error of the average values are smaller than 0.2 for salinity and 1 °C for temperature. The pair values vary along the $x = y$ identity line, although a small angle of the linear fit was computed for salinity and a small shift due to higher simulated values was computed for temperature. Both differences are related to the deep-water mass detected at Station S3 in October 2017 (Figs. 5 and 6) that was characterized by high salinity and low temperature. The model overestimated the temperature and underestimated the salinity for this water mass; however, the model efficiently reproduced this dense ASW intrusion a few kilometres (~5 km) south of Stations S3, as discussed in Section 4.2 (see Fig. 16c and d). The T/S diagram (Fig. 8c) shows good agreement between model and observations for both stratified and homogenous water columns. The density differences between observed and simulated values (Fig. 8d) are very small in all stations, Average S1 = 0.37, S2 = 0.24, S3 = 0.49 for the central-, inner-, and outer-Gulf, respectively. The latter is related to the deeper water mass of October. Generally, the simulated density is slightly smaller than the observed density (positive error; Fig. 8d), related to the small overestimation of the simulated temperature (Fig. 8b). The error increases with depth and it is higher for Station S3 due to the simulated salinity underestimation in the deeper layers (below 15 m) as previously discussed.

The horizontal distributions of temperature and salinity derived from
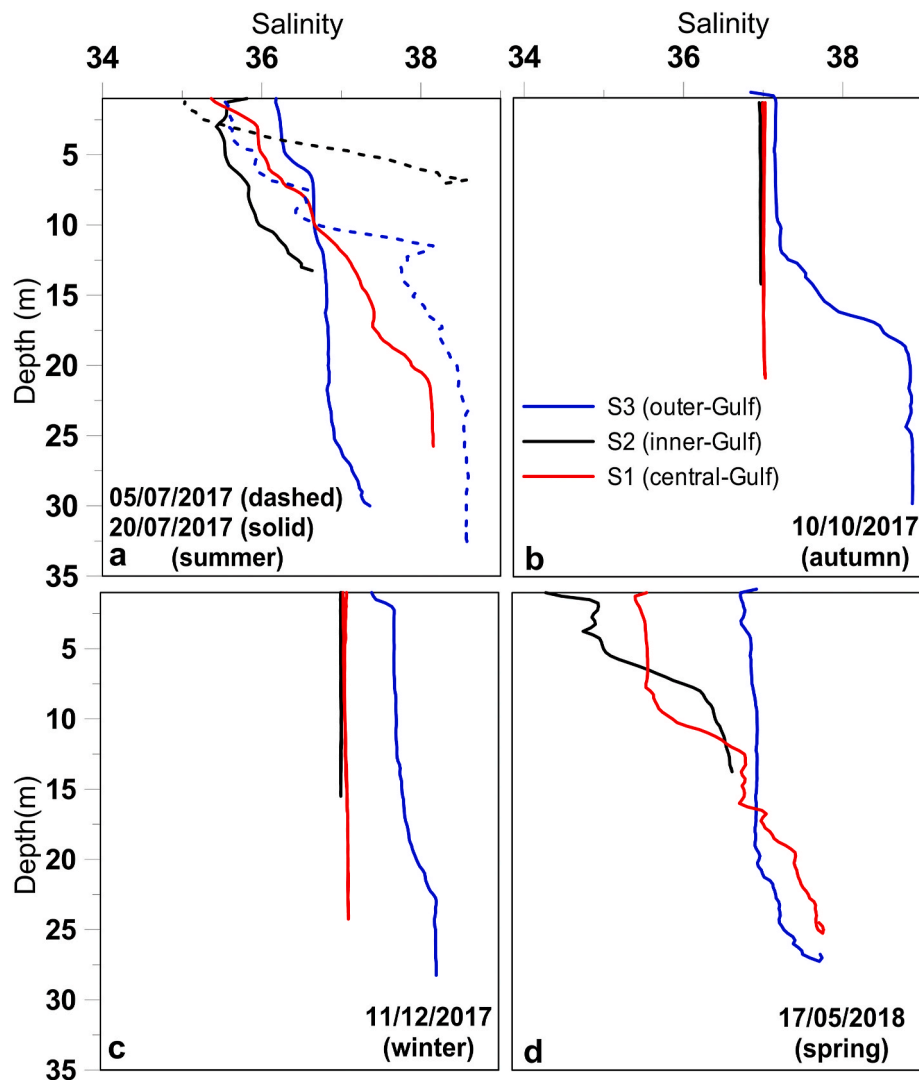
Fig. 6. Vertical profiles of salinity (CTD) at S1 (red line), S2 (black line), S3 (blue line) stations on (a) 05/07/17, 20/07/17, (b) 10/10/17, (c) 11/12/17, and (d) 17/05/18. Measurements at Station S1 on 05/07/17 were not available.

the Delft3D-Thermaikos simulation are presented in Fig. 9. All cases agree with the SST distribution derived from the GHRSST fields (Fig. 7); warmer water masses were simulated over the inner-Gulf in early-July when strong southerly winds prevailed over the entire NTG (Fig. 9a). The southerly winds induced a general northward spreading of surface waters imposing an anticyclonic circulation. The surface salinity revealed smaller values in the inner- and central-Gulf (35; Fig. 9b) than the outer-Gulf (36.5; Fig. 9b) in agreement with the *in situ* observations collected on July 5 in Stations S2 and S3, respectively. Two distinct circulation features emerged from the surface current fields; an anticyclonic pattern in the central- and inner-Gulf and a second anticyclonic eddy in the outer-Gulf, keeping the two water masses separated. A similar anticyclonic circulation pattern prevailed in the central-Gulf a few days later (Fig. 9d), on July 20, under weak northerly winds (Fig. 9c), with smaller river discharge rates (Fig. 1b) and limited spreading of brackish waters, especially over the central-Gulf. Stronger northerly winds, that prevailed in mid-July (Fig. 7b; see also Section 4.2), played a role on the southward advection of the riverine plume, away from the northern central- and inner-Gulf regions (Fig. 9d). A different circulation pattern predominated between 5 and 20 July in the inner-Gulf; southwestward currents increased the salinity levels in the eastern part of this region (Fig. 9b) in agreement with the *in situ* measurements (Station S2; Fig. 6a). A water mass with higher salinity values,

that was previously (July 5) detected only in the southern outer-Gulf, spread more to the north, moving the density front closer to the central-Gulf on 20 July (Fig. 9d). All regions of the Gulf, except from the ones in the vicinity of the river mouths (southwestern NTG), revealed higher salinity values (>36; Fig. 9d) than the previous study case. The small period of strong northerly winds that occurred in mid-July played a role on the different eutrophication levels and physical distribution between the two campaigns (see Section 4).

Significantly strong northerly winds (>10 m/s; Fig. 9e) prevailed in October over the entire study region imposing a respective southwestward spreading of surface waters with currents higher than 0.5 m/s (Fig. 9f). Both satellite and Delf3D-Thermaikos SST values ranged around 21 °C with slightly colder waters at the southeastern outer-Gulf, south of Station S3. The strong winds also promoted the mixing of the water column (Figs. 5b and 6b), and the increase of the surface salinity in the entire NTG (37; Fig. 9f).

During the eutrophication event in early-winter 2017 (11/12/17), the prevailing southerly winds (Fig. 9g) induced a respective northward surface circulation pathway (Fig. 9h). The simulated SST distribution agrees with the satellite GHRSST values (Fig. 7d) indicating two separate water masses between the inner- (colder and less saline) and outer-Gulf (warmer and saltier) as also derived by the field observations (Figs. 5c and 6c). Although southerly winds may drive surface waters
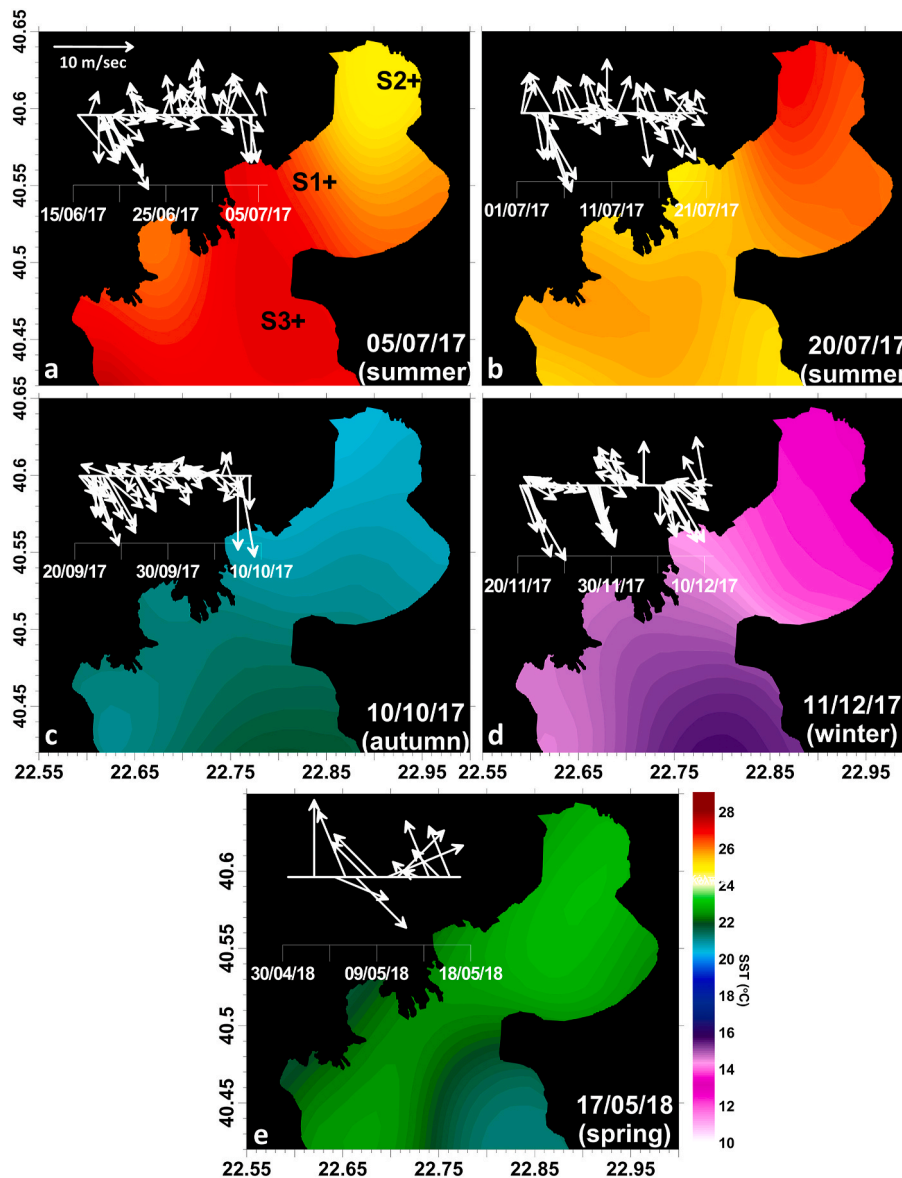
Fig. 7. Horizontal distribution of Sea Surface Temperature (SST; °C), derived from the GHRSST database during the seasonal observational campaigns in Thermaikos Gulf on (a) 05/07/17, 20/07/17, (b) 10/10/17, (c) 11/12/17, (d) 17/05/18 and (e) 17/05/18. Wind vectors (m/s) for 20 days prior to each observational campaign, collected by the AUTh meteorological station, are overlaid at each SST map.

towards the North, they can also confine the inner-Gulf surface waters and enhance eutrophication phenomena especially when riverine brackish waters are trapped in the northern part of the NTG.

4. Discussion

The prevailing circulation dynamics related to the meteorological conditions, the exchanges with the open sea, and the river outflows (Krestenitis et al., 2012), control the main circulation pathways and the connectivity between sub-regions inside the NTG. We hereby examine the main circulation features that control the connectivity pathways which may lead to either favorable conditions for the formation of eutrophication phenomena or contribute to the renewal of the northern NTG.

4.1. Ocean dynamics during eutrophication events

The evolution of the velocity components of near-surface (1st model sigma-layer) and deeper (12th model sigma-layer; ~15 m) currents,

vertical to the center of Sections 1 and 2 before, during, and after the two eutrophication events (dirty sea in late-June and early-July, and red tide in December) are presented in Figs. 10 and 11. The strong southerly winds that prevailed the week before the observational campaign on July 5 (dirty Sea event; Fig. 10a) coincide with northeastward near-surface currents and southwestward currents at 15 m across Section 1 (~0.1 m/s; Fig. 10b). Similar northward currents are also apparent in the general anticyclonic circulation presented in Fig. 9b that reduced the inner-Gulf salinity (Fig. 6a) due to the northward spreading of the brackish river waters, discharged mainly by Aliakmonas river in end-June (Fig. 1b). The inflow (into the central-Gulf) and outflow (into the outer-Gulf) transport via Section 1 is relatively small (<4000 m^3/s; Fig. 10d) until July 3, indicating weak exchanges of water masses and minimal renewal of the northern parts of the NTG. The respective exchange across Section 2 (between inner- and central-Gulf) is also minimal (thin lines in Fig. 10d). The evolution of the renewal time in the area that includes the central- and inner-Gulf regions was computed based on the ratio between the volume of the area north of Section 1 (2.12 × 10^9 m^3) and the inflow transport hourly rate. High transport rates are
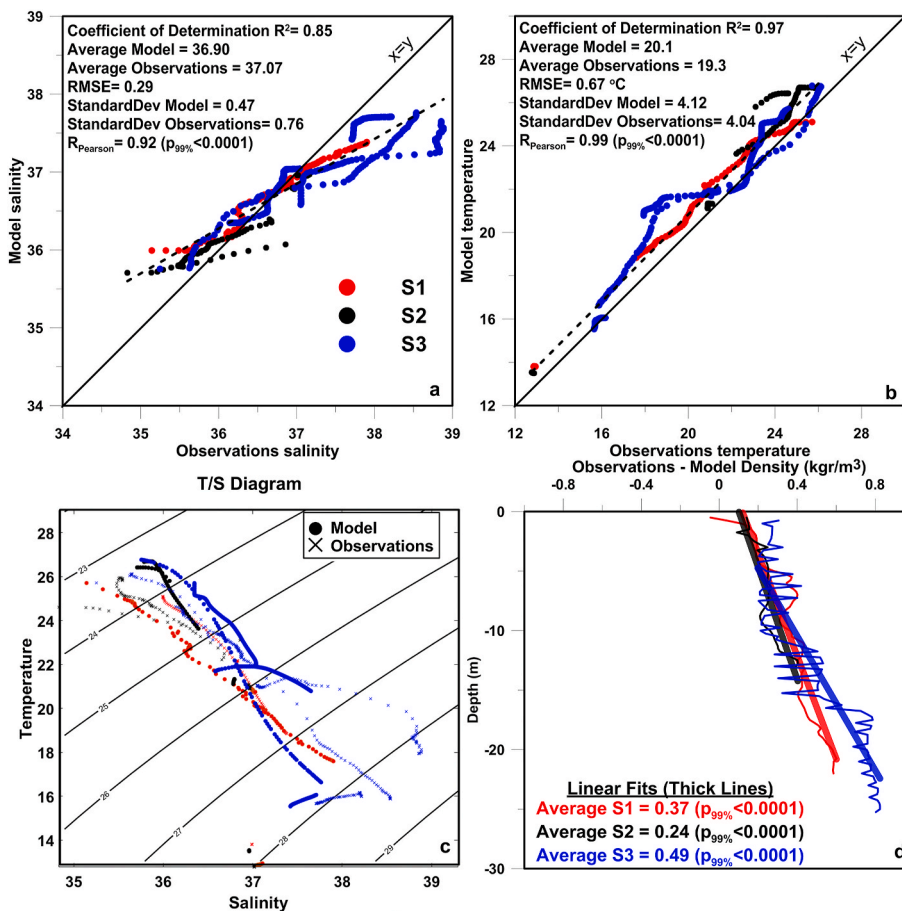
Fig. 8. Scatter diagram between simulated and observed (a) salinity and (b) temperature derived at Stations S1, S2 and S3 for 05/07/17, 20/07/17, 10/10/17, and 11/12/17. The coefficient of determination R^2, the average values, the Root Mean Square Errors (*RMSEs*), the standard deviations (*StandardDev*), and the Pearson correlation coefficients ($R_{Pearson}$) with the respective statistically significance $p_{99\%}$ test are presented for each scatter diagram. (c) T/S diagram of all stations (3 colors), sampling depths and dates of simulated (● symbol) and observed (× symbol) values. (d) Vertical distribution of the mean differences between the observed and simulated density (errors) at all depths (thin lines). The respective linear fits (thick lines) with the average error values and the statistically significant test of each fit ($p_{99\%}$) for all depths and dates for each station are also presented.

associated to a faster renewal of the semi-enclosed region while weak transports may lead to slower renewal lasting larger periods. An increase of renewal time (30 days; Fig. 10e) occurred around July 3 due to respective minimal transport exchange (Fig. 10d). A respective increase was computed for the inner-Gulf (3.65×10^8 m^3) during the same period (Fig. 10e). An increase of transport (6000 m^3/s) and a respective reduction on the renewal time (5 days) was computed around July 5 (Fig. 10d) due to a very short period (1.5 days) of northerly winds (Fig. 10a). The latter induced a reversal of the surface current directions along both Sections 1 and 2 around July 4 (Fig. 11a and b). The short duration of this circulation pattern was not able to weaken the eutrophication - dystrofication event that formed during the previous period. Southerly winds and northeastward currents at the central-Gulf dominated again until mid-July, reducing the transport rates (Fig. 10d) and increasing the renewal times (>20 days; Fig. 10e). A renewal event that occurred after July 16 (see Section 4.2) improved the water quality of the central- and inner-Gulf, reducing the chl-a concentrations derived from the satellite data and averaged over the areas north of each Section (Fig. 10e).

In December 2017, northerly winds prevailed between December 4 and 9 (Fig. 11a) inducing southward surface currents across Section 2 (Fig. 11c) and almost zero currents across Section 1 (Fig. 11b). This period was characterized by a southward spreading of freshwaters with high chl-a concentrations, originated from Axios River (Fig. 3d). Winds weakened after December 7 and finally changed from northerlies to southerlies on December 9 (Fig. 11a), when the phytoplankton biomass (Fig. 2c) and chl-a concentrations significantly increased as derived from both satellite (Fig. 11e) and *in situ* measurements (Fig. 2c). The general circulation over the central- and inner-Gulf (Fig. 9h) agrees with the surface currents computed across Sections 1 (Figs. 11b) and 2 (Fig. 11c) during the dominance of southerly winds. The respective deeper

currents at 15 m were weak but southward across Section 1 (Fig. 11b). Generally, surface (northward) and deeper (southward) currents were very weak across Section 2 on December 10 (Fig. 11c). The inflow and outflow transports were significantly small (~1000 m^3/s; Fig. 11d) before December 10 and increased to 5000 m^3/s on December 10. However, this increase is related to stronger inflow over the upper layers and outflow in the deeper layers of Section 1 in agreement with the respective variation of the near-surface and 15 m current velocities. The winds changed again to northerlies (Fig. 11a) reducing the current speeds on December 10 and 11 (Fig. 12b and c). The small exchange mainly across Section 1 (Megalo Emvolo) during the first 10 days of December was associated to large renewal times (Fig. 11e) consisting favorable conditions for the formation of the red tide event (Fig. 4b) detected on December 11 (Figs. 2c and 3e). Similarly, the transport across Section 2 (Mikro Emvolo) reduced after December 7 increasing the respective renewal time in the inner-Gulf. In severely eutrophicated regions of the inner-Gulf (Fig. 2c), the highest renewal time of the first 20 days of the month was computed on December 9, when the winds reversed from northerlies to southerlies after two days (December 7–8) of continuous decrease in magnitude (Fig. 11a). This reduction and the final reverse of the wind direction led to the reduction of the southward flow across Section 2 from 4000 m^3/s on December 6 to 1000 m^3/s on December 9 (Fig. 11d). The seawater quality of the Gulf was significantly improved by December 20 (Figs. 3f and 11e) after a period of persistent northerly winds between December 16 and 20 (Fig. 11a). The latter conditions induced southward surface currents in the inner- (Fig. 11c) and central-Gulf (Fig. 11b), and increased the inflow transport, especially between central- and inner-Gulf (Section 2; Fig. 11d). A renewal time increase was computed for the inner-Gulf on December 15 under southerly winds and a respective time reduction after December 16 under northerly winds.
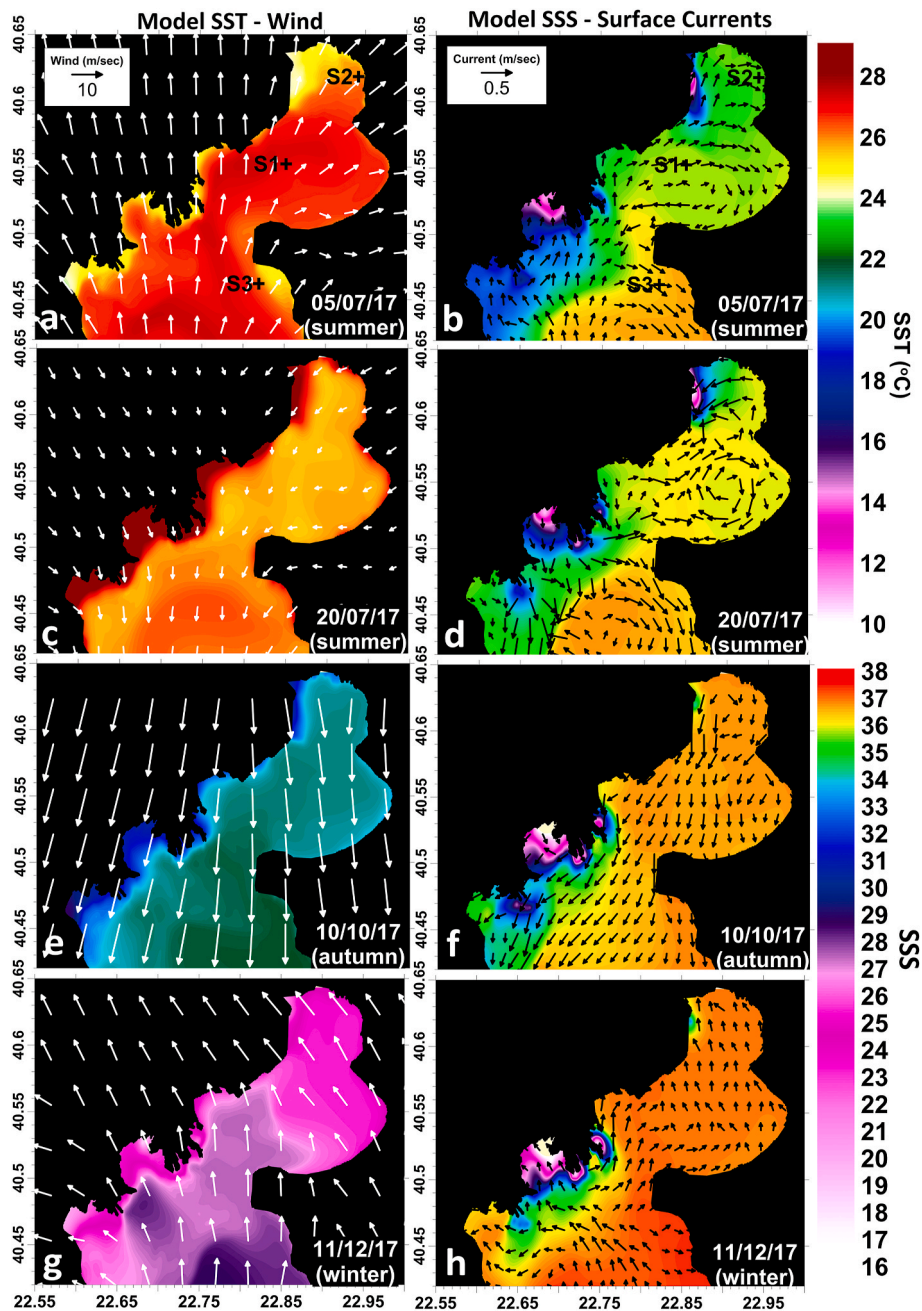
Fig. 9. Horizontal distribution of Sea Surface Temperature (SST; °C) and Sea Surface Salinity (SSS), derived from the Delft3D-Thermaikos simulations, overlaid with wind vectors (WRF-METEO-AUTh; m/s) and simulated surface current vectors (m/s), respectively on (a)–(b) 05/07/17, (c)–(d) 20/07/17, (e)–(f) 10/10/17 and (g)–(h) 11/12/17.

4.2. Ocean dynamics during renewal events

4.2.1. Temporal evolution

Strong northerly winds (>10 m/s) occurred between July 16 and 20 (Fig. 10a) that enhanced the southward surface currents (0.15 m/s) in the central- (Fig. 10b) and inner-Gulf (Fig. 10c). Strong deeper northward flows occurred across Section 1 and towards the central-Gulf (Fig. 10b). The respective inflow and outflow across Section 1 were larger than 6000 m^3/s (Fig. 10d) reducing both the renewal time of the northern regions of NTG (<5 days) and the chl-a mean values (<4 mg/ m^3; Fig. 10e) in agreement with the *in situ* values (Fig. 2a). Similar variations of transport and renewal time were computed for Section 2 (inner-Gulf). These meteorological and oceanic conditions contributed to the renewal of the NTG and improved the water quality (clear waters

state).

A case of clear waters was also identified around October 10 after a period of strong northerly winds (15 m/s; Fig. 12a) that also increased the southward velocities of the surface currents (>0.15 m/s) in both the central- (Fig. 12b) and inner-Gulf (Fig. 12c); the bottom currents across Sections 1 and 2 revealed a clear northward component indicating a two-layer flow that contributes to the northward intrusion of open sea waters over the deeper layers. Large exchange transport rates were computed across Sections 1 and 2 (>3500 m^3/s; Fig. 12d) between October 6 and 9, reducing the renewal times to 3 days for the inner-Gulf (thin line in Fig. 12e) and to 10 days for the inner- and central-Gulf combined (thick line in Fig. 12e). The renewal time increased after October 10 (~30 days), when southerly winds (Fig. 12a) and north-eastward surface currents prevailed, especially across Section 1
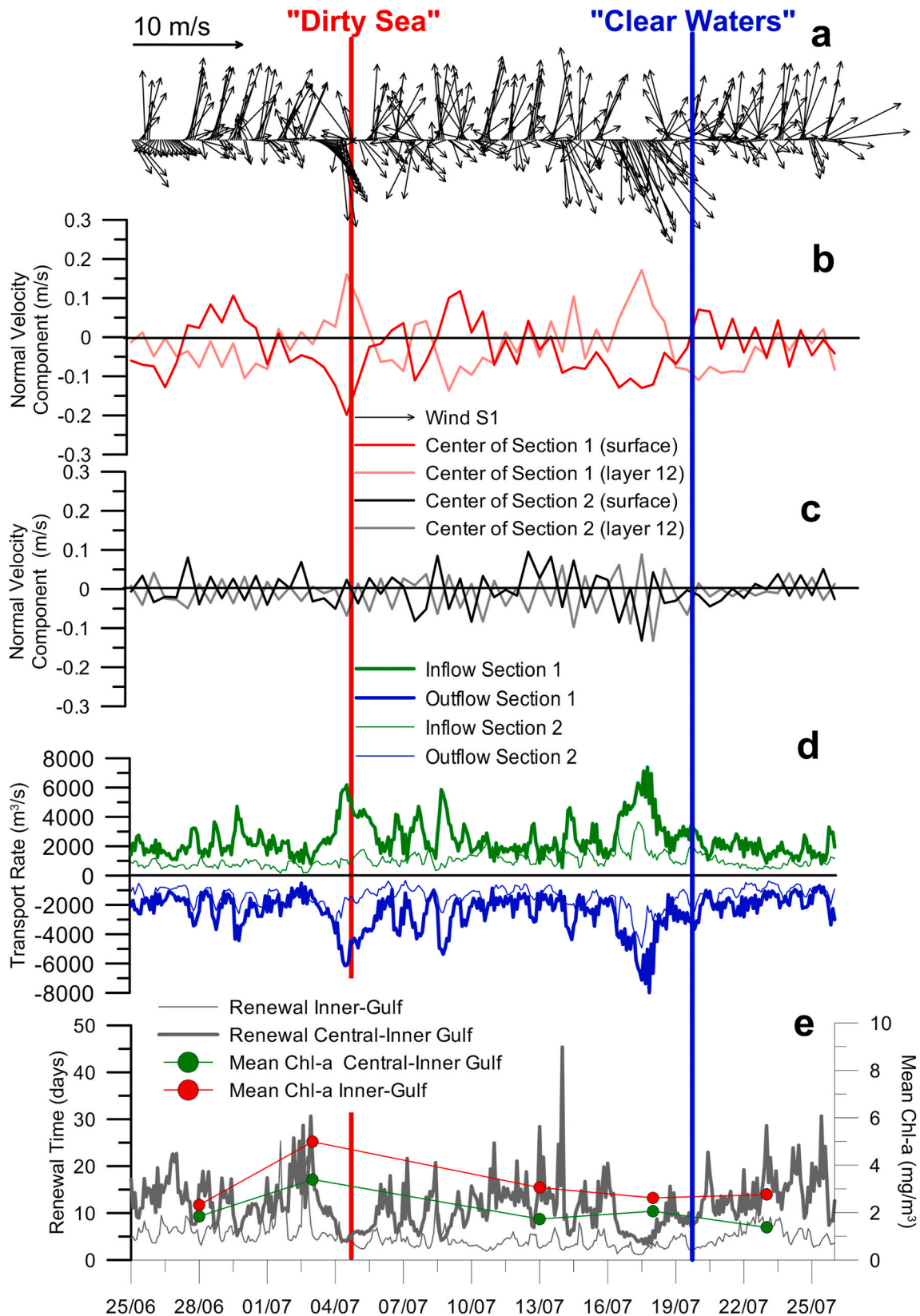
Fig. 10. Hourly evolution of (a) wind vectors (m/s) at Station S1, normal current component of the 1st (surface) and 12th (~15 m) model layer (Delft3D-Thermaikos; m/s) at (b) the center of Section 1 (red and pink lines) and (c) center of Section 2 (black and grey lines), and (d) inflow transport (positive; green line), outflow transport (negative; blue line), and (e) renewal time (grey line) across Sections 1 (thick lines) and 2 (thin lines) as derived from Delft3D-Thermaikos simulation between 25/06/17 and 26/07/17. The chl-a concentrations derived from the available Sentinel-2 and Sentinel-3 images and averaged over the area north of Section 1 (Inner- and Central-Gulf) and Section 2 (Inner-Gulf) are also shown with green and red color lines in (e). The dates that the "Dirty Sea" (red line) and "Clear Waters" (blue line) events were detected are marked with vertical lines. Positive (negative) velocity and transport values are associated to northward (southward) direction.
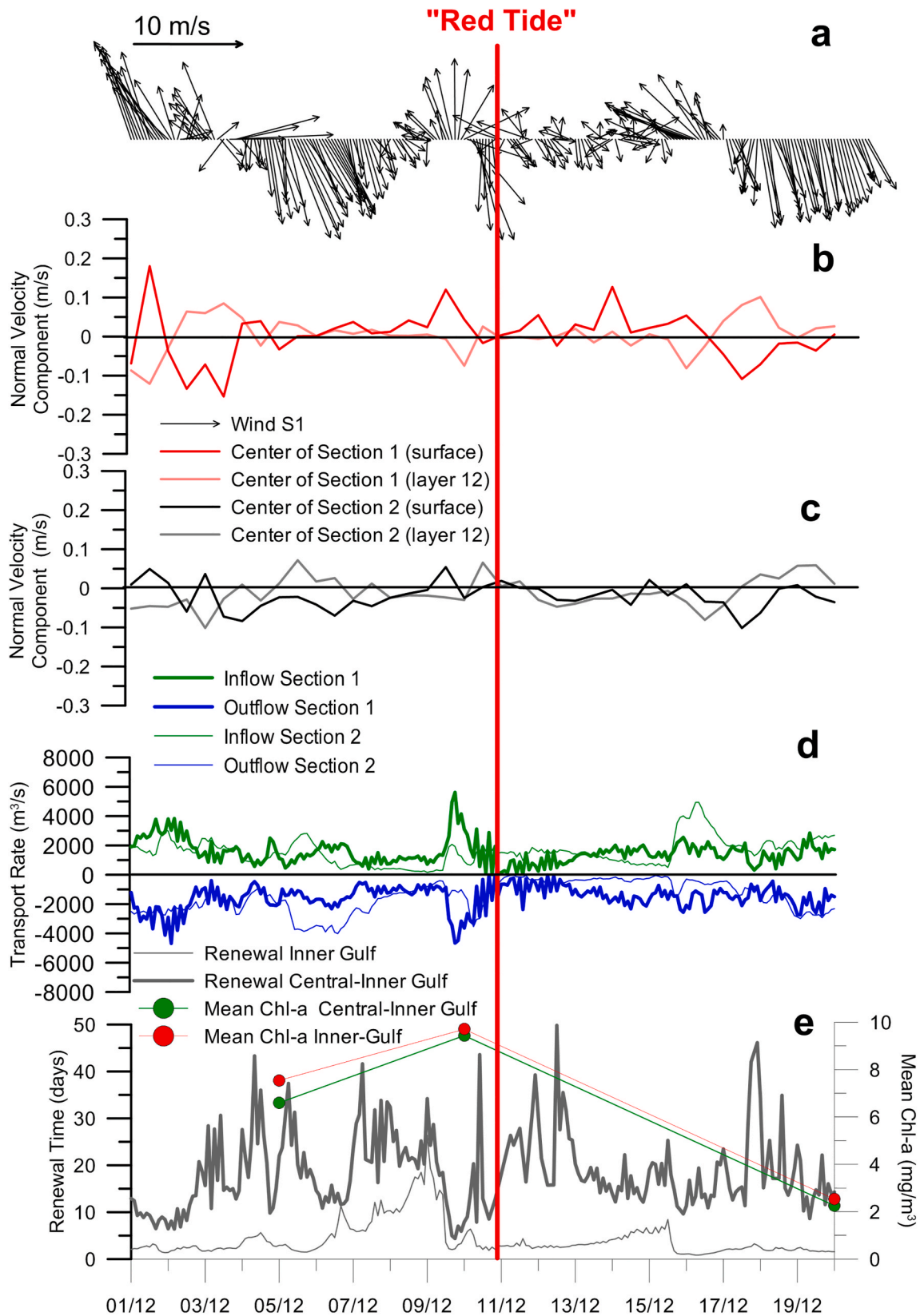
Fig. 11. Same as Fig. 10 but from 01/12/17 to 20/12/17. The date that "Red Tide" (red line) event was detected is marked with a vertical line.

(Fig. 12c). The northerly winds in mid-October reversed the direction of the surface and deep currents again. Thus, they increased the outflow (southwestward) and inflow (northeastward) transports, respectively, reducing the renewal time of the northern NTG (2 days for inner-Gulf

and 10 days for the two northern regions together; Fig. 12e).

The effect of the northerly winds on the exchange transports between the Gulf's regions and the open sea is apparent during the entire period from July to December 2017 (Fig. 13). The variability of the meridional
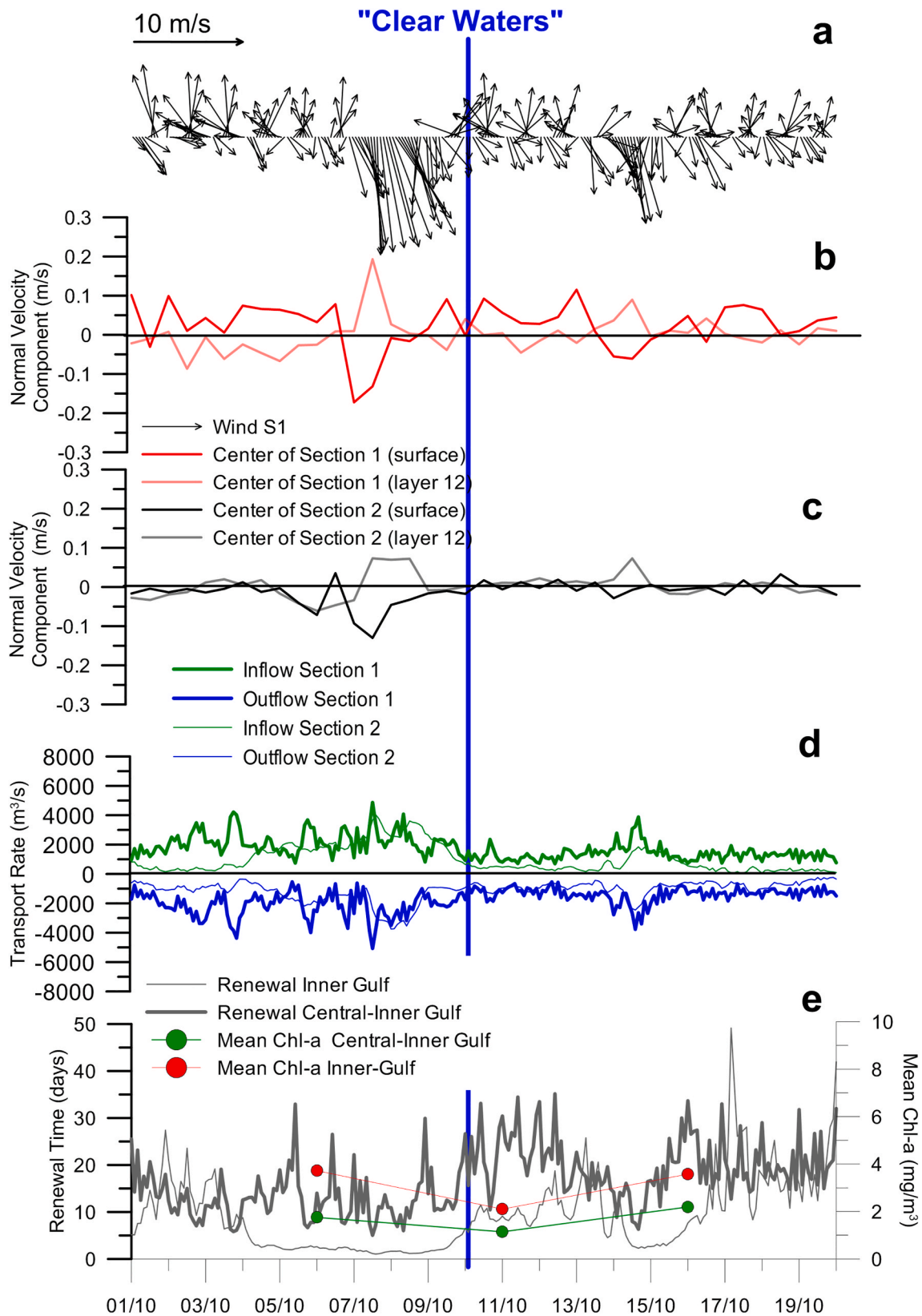
Fig. 12. Same as Fig. 10 but from 01/10/17 to 20/10/17. The date that "Clear Waters" (blue line) event was detected are marked with a vertical line.

component of the wind (W_y) across Section 1 (Figs. 13a) and 2 (Fig. 13b) coincides with the variation of the renewal time of the area located north of each section. There are yet a few periods that southerly (positive W_y) and northerly (negative W_y) winds can be associated with short (strong

exchange transport) and long (weak exchange transport) renewal periods, respectively. However, the polynomial fit of 5th order, computed for each month, shows the same variation for W_y and renewal time; short renewal periods under northerly winds long renewal periods under
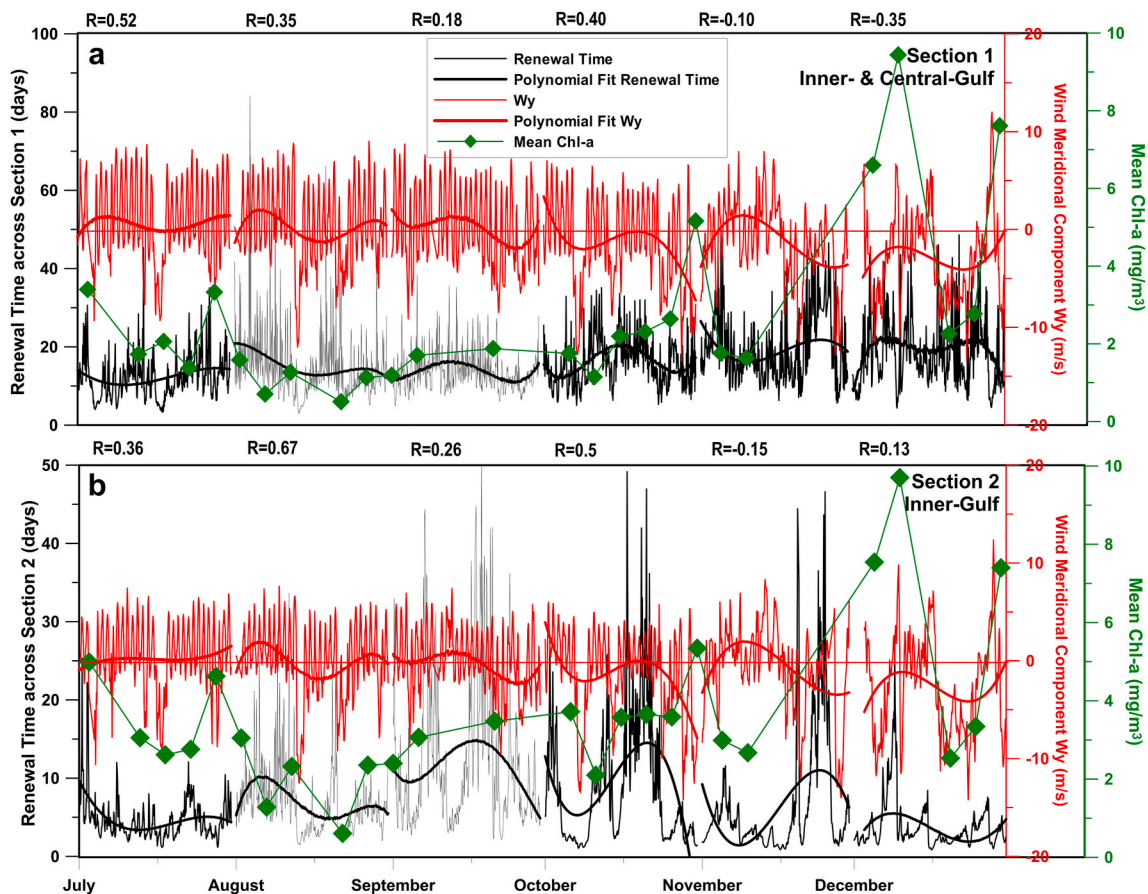
Fig. 13. Evolution of renewal time (black line; refer to left y-axis) computed for the area northern of (a) Section 1 and (b) Section 2 between July and December 2017. The respective evolution of the meridional component of the wind W_y (m/s) at the center of each section is presented with red line (refer to right y-axis). The monthly 5th order polynomial fits for each variable are also shown with thick lines. The chl-a concentrations derived from the available Sentinel-2 and Sentinel-3 images and averaged over the area north of (a) Section 1 (Inner- and Central-Gulf) and (b) Section 2 (Inner-Gulf) are also shown with green lines. Six values of Pearson correlation coefficients (R) between W_y and renewal time are presented for each month. Note that the renewal time scale (left y-axis) is different between (a) and (b) for clarity reasons.

southerly winds. The temporal distribution of the mean chl-a concentrations for each area generally follows the variation of the renewal time with high and low values during long and short renewal periods. The match is better in the inner-Gulf (Fig. 13b) that revealed generally higher monthly correlation coefficients, where the variations of the fits are the same between wind and renewal time during all months, except from November (negative correlation coefficient). Even though, two very strong northerly wind events in mid-November were strongly related to a very large decrease of the renewal time, especially of the inner-Gulf (Fig. 13b). Most of the monthly Pearson coefficients are positive and statistically significant for both regions ($p_{value} < p_{95\%} = 0.05$). However, small or even negative coefficients were also computed (e.g., November); the circulation patterns that determine the computed renewal time are not always related to the prevailing meteorological conditions since the effect of other processes is also important (e.g., exchanges with the open sea, river-plume dynamics, thermohaline circulation etc).

4.2.2. Vertical structure

The southwestward spreading of the NTG's surface waters during the renewal event of October was detected at the upper 10 m of Section 1 (Fig. 14b). On October 7, the southwestward moving upper layer was very thick with strong velocities (0.15 m/s; Fig. 14b) at the west side of the passage (along the Axios Delta) that connects the central-with outer-Gulf. Similarly, northeastward currents occurred between 10 and 20 m

of depth. Especially at the east side of the passage, the thickness of this layer is even larger (5 m to bottom), confirming the cyclonic circulation that may improve the renewal of the NTG in agreement with Hyder et al. (2002) and Krestenitis et al. (2012). On October 10, a strong northeastward flow was detected in the deeper layers of the eastern part of Section 1, along Megalo Emvolo peninsula, indicating the inflow of deeper open sea waters into the central-Gulf (Fig. 14c). On the contrary, the near-surface layer was characterized by clear northward currents a few days earlier (e.g. on October 5; Fig. 14a), when weak but southerly winds prevailed (Fig. 12a). The northward flow between the inner- and central-Gulf (Section 2) was stronger on October 7, covering almost the entire central and eastern parts of the passage (Fig. 14e). Simultaneously, very strong southward flows (~0.15 m/s) occurred along the western coasts associated to the general cyclonic circulation. This is not the case on October 5, when very weak currents (<0.05 m/s) prevailed across the entire Section S2 (Fig. 14d). The cyclonic circulation was still apparent on October 10 with southward and northward currents along the western and eastern side of the passage, respectively (Fig. 14f).

Field current measurements, that were conducted at Stations S1 and S3 on November 14, 2019, confirmed the two-layer circulation that usually prevails under the influence of northerly winds (Fig. 15). Southward currents were observed over the upper 5 m, while northward flow towards the northern NTG was detected between 17 and 25 m of depth (Fig. 15a). A similar velocity distribution was also measured at the southern Station S3 with near-surface southward currents and northward flows between 7 m and the bottom of Station S3 (Fig. 15b). The
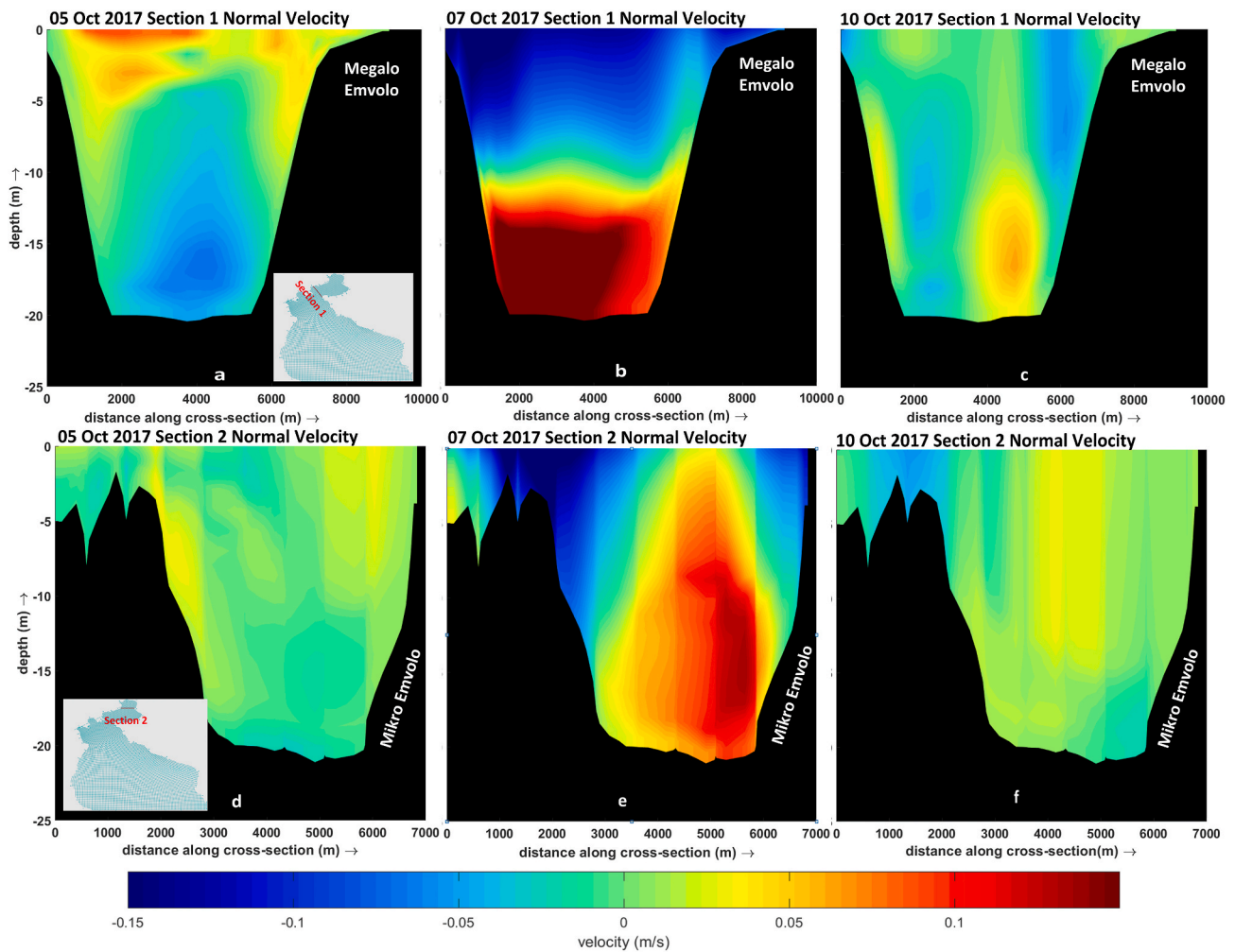
Fig. 14. Vertical distribution of normal velocity (m/s) on (a) 5/10/17, (b) 7/10/17, (c) 10/10/17 across Section 1 and (d) 5/10/17, (e) 7/10/17, (f) 10/10/17 across Section 2, as derived by the Delft3D-Thermaikos simulation. Sections 1 and 2 are marked on the insert maps at panels (a) and (d), respectively. The eastern land boundary of each Section is marked with the respective topography feature (Megalo Emvolo for Section 1 and Mikro Emvolo for Section 2; Fig. 1a).

ocean color image, collected on the same date, confirms the relatively good quality of the central-Gulf in terms of chl-a concentrations during these met-ocean conditions (northerlies driving surface outflow with deep inflow).

The intrusion of cold and more saline Aegean waters, especially along the eastern coasts of the NTG, detected by the *in situ* observations at Station S3 in October 2017 (Figs. 5b and 6b), plays a significant role on the increase of the water mass exchange between the inner-, central-, and outer-Gulf regions. A colder (<20 °C; Fig. 16b) and more saline (~38.5; Fig. 16d) water mass was detected along the eastern coast between Station S3 and the southern boundary of the model domain on October 10, 2017. The upper layers at the northern part of Section 3 are occupied by a water mass with lower salinity (<37) and higher temperature (21 °C) than the near-bottom layers. The simulated results agree with the field data collected in Station S3 (Figs. 5b and 6b), showing a strong deep pycnocline between 17 and 20 m. The different circulation pattern 5 October 5, when southerly winds prevailed, was also depicted on the distribution of temperature and salinity values along the eastern coast (Fig. 16a and c). The deep ASW tongue that expanded northward along the eastern coast on October 10 (~5 km south of Station S3), was significantly retracted to the South (~30 km south of Station S3) on October 5. In particular, the northern part of Section 3 (40.45°N) was characterized by warmer waters (~22 °C; Fig. 16a) with lower salinity values (~36.5; Fig. 16b).

5. Conclusions

The conspicuous eutrophication events in a typical, microtidal, semi-enclosed, coastal inlet of the Euro-Mediterranean coastal zone (Northern Thermaikos Gulf; NTG) were investigated and associated to fine-scale ocean circulation features during an annual cycle. New insight is provided on mesoscale and sub-mesoscale effects of ocean circulation on nutrient-rich freshwater discharges by a multi-river inlet mainly responsible for HABs. Field observations in tandem with satellite data and numerical simulations depicted the prevailing ocean conditions during the formation of eutrophication phenomena. This integrated approach allowed the investigation of the contribution of the physical processes on the water renewal and quality of the Gulf. The *in situ* observations and the satellite data confirmed the efficiency of the high-resolution Delft3D-Thermaikos model to simulate the hydrodynamic circulation in the NTG, a semi-confined microtidal coastal area that is mainly affected by local weather conditions and strong river discharges with respect to physical, chemical, and biological properties of seawater. Ocean color satellite data provided information with high spatial and temporal resolution over the entire NTG and are used to identify the pathways of the brackish waters and the accompanying eutrophication phenomena in shallow coastal areas of the NTG.

The eutrophication events (e.g., "Dirty Sea mucilaginous aggregates" in June–July 2017 and "Red Tide" in December 2017), described in the study, were mainly associated with the dominance of southerly winds,
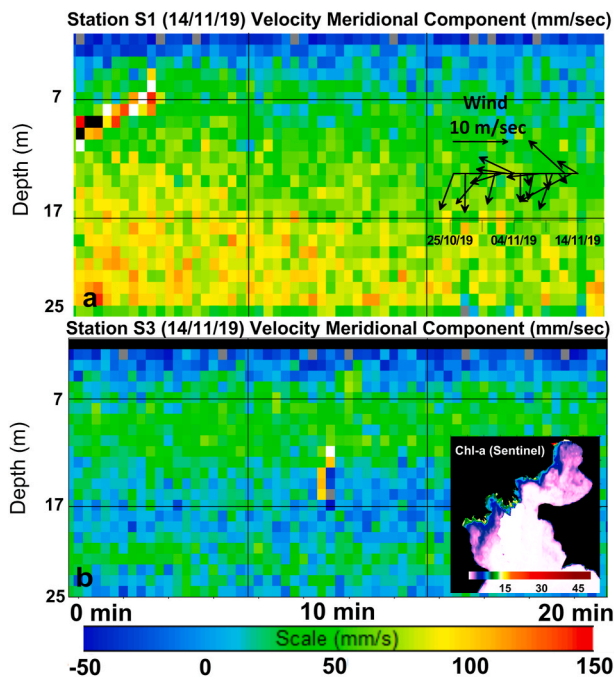
Fig. 15. Vertical distribution of the meridional (North-South) component of current velocity, measured with ADCP at Stations (a) S1 and (b) S3 for 20 min on 14/11/19. Measured wind vectors (m/sec) for 20 days prior to the ADCP campaign are overlaid at panel (a). The respective surface chl-a concentrations (mg/m^3), derived from the Sentinel-2 satellite data, are presented in the insert of panel (b).

which affect the ocean circulation over the NTG in three ways:

1) They confine the surface waters in the northern parts of the NTG (central- and inner-Gulf) separating the waters masses between the northern and southern regions,
2) They contribute to the northward spreading of nutrient-rich brackish waters towards the northern parts of the Gulf, originated from the main rivers of Thermaikos (Axios and Aliakmonas). The

phytoplankton species of the different habitat communities of S1, S2 and S3 were highly connected while S1, located closer to the river deltas showed the largest species pool including nutrient opportunists (Vallina et al., 2014).

3) They impose an anticyclonic circulation, especially in the inner- and central-Gulf weakening their renewal process, which is mainly associated with cyclonic circulation that supplies the NTG along the eastern coasts with clearer Aegean Sea Waters (ASW; Hyder et al., 2002; Krestenitis et al., 2012).

The renewal events were related to northerly winds that enhance the spreading of the coastal waters and dispersing abundant phytoplankton towards the southern parts of the NTG (outflow) and eventually towards the open sea of the Aegean. It is likely to connect distant phytoplankton communities influencing their local dynamics (Moritz et al., 2013). The northerly winds also removed polluted and nutrient-rich brackish waters away from the enclosed northern NTG regions. Under these met-ocean conditions, a northward pathway of ASW is formed in the deeper layers (inflow), especially along the eastern coast, extending the general cyclonic circulation of the North Aegean Sea (Zervakis and Georgopoulos, 2002; Androulidakis and Kourafalou, 2011; Androulidakis et al., 2012) into Thermaikos Gulf. Under this two-layer flow, waters originated from the open sea were detected in the inner parts of the NTG, imposing unfavourable conditions for the formation of extended eutrophication events.

The knowledge of the transport exchange rates along the passages between the central- and outer-Gulf (Megalo Emvolo to the East and Axios River to the West) and between the central- and inner-Gulf (Thessaloniki Bay) showed that these are unique control areas to identify the renewal conditions of the NTG. The feeble exchange is associated to weak renewal (high renewal time periods) and isolation of water masses in the central and inner parts of the NTG (eutrophication-favorable conditions). On the contrary, large exchange with strong southward upper-layer flows and northward lower-layer flows, indicates strong renewal (small renewal time periods) which in synergy with strong northerly winds leads to the mixing of the water masses, improving the seawater quality (clear waters periods) in the NTG.

Although the eutrophication state of the NTG is mainly determined by ecological and biogeochemical processes (Dutkiewicz et al., 2009; Sommer et al., 2018; Genitsaris et al., 2019), we also showed that the
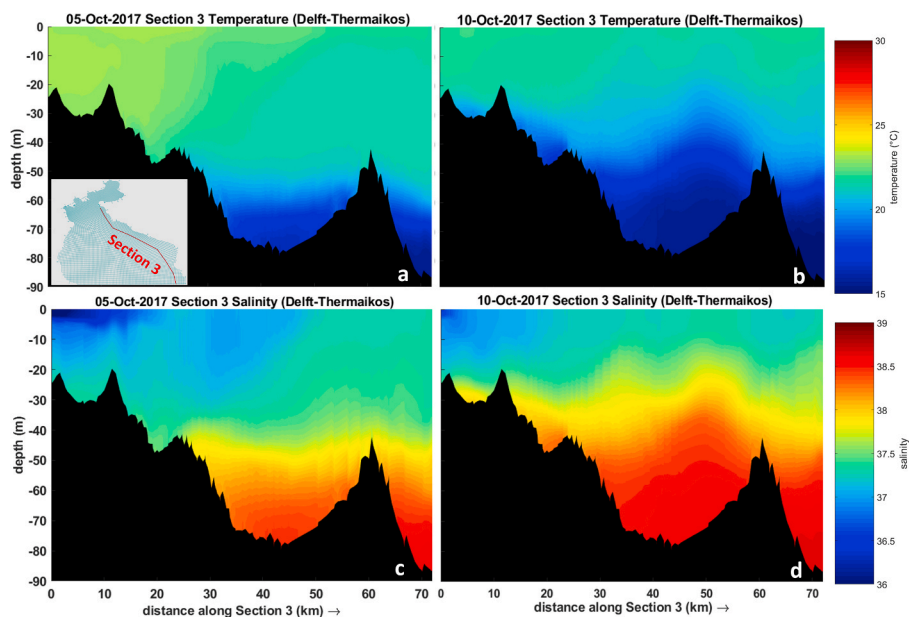
Fig. 16. Vertical distribution of temperature (°C) on (a) 5/10/17, (b) 11/10/17, and salinity on (c) 5/10/17, (d) on 10/10/17 along Section 3, as derived by the Delft3D-Thermaikos simulation. Section 3 is marked in the insert map of panel (a).

localized-scale ocean dynamics may provide favorable conditions for the formation or amplification of such events by either reducing the renewal of the Gulf with clear waters or by advecting nutrient-rich waters from the rivers to the northern coastal areas. Moreover, connectivity enhances fluvial translocation of opportunistic phytoplankton forming eutrophication episodes, thus leading different habitat communities to be highly connected. Ocean circulation shapes marine phytoplankton communities by setting environmental conditions and dispersing microorganisms (Kuhn et al., 2019). Therefore, the physical properties of coastal waters and the fine-scale hydrodynamic circulation should be considered when investigating the formation of eutrophication events, especially in rather shallow, semi-enclosed, river-impacted, microtidal gulfs of the Euro-Mediterranean continental shelf. Near-future forecasts of the hydrodynamic circulation with valid and updated river outflow rates in tandem with continuous field and satellite monitoring should be included in a real-time operational system for the prediction of such hazardous events before their formation. The synergy of physical, ecological, and biogeochemical effects on the formation of eutrophication events in Mediterranean coastal areas is a very interesting topic, with high socio-economic and environmental implications (Pinardi et al., 2006) and requires further investigation. The process-oriented study at hand aims to contribute to this field, focusing on a regionally important enclosed coastal ecosystem, the Northern Thermaikos Gulf, that concentrates almost all aspects of modern human activities in its vicinity. Establishing met-ocean conditions and circulation patterns that favor or mitigate eutrophic conditions under renewal processes should be an important component of a successful coastal zone management strategy. The methodology and findings described in the manuscript can be applicable to analogous coastal areas worldwide and serve as a helpful guide in approaching the multidisciplinary issue of coastal eutrophication.

Declaration of competing interest

The authors declare that they have no known competing financial interests or personal relationships that could have appeared to influence the work reported in this paper.

Data availability

Data will be made available on request.

Acknowledgments

References

Alexandridis, T.K., Monachou, S., Skoulikaris, C., Kalopesa, E., Zalidis, G.C., 2015. Investigation of the temporal relation of remotely sensed coastal water quality with GIS modelled upstream soil erosion. Hydrol. Process. 29 (10), 2373–2384.

Androulidakis, Y., Moustaka, M., Darakas, E., Petala, M., Tsiridis, V., Makris, C., Stefanidou, A., Antoniadou, Ch, Genitsaris, S., Baltikas, V., Ramnou, D., Chintiroglou, C., Krestenitis, Y., 2018. Observational study of the marine environment in the northern Thermaikos gulf. In: Proc. Of the 12th Pan-Hellenic Symposium of Oceanography and Fisheries, Hellenic Center of Marine Research, Ionian University, Corfu, Greece, 30 May - 3 June 2018, ISBN 978-960-9798-08-2, p. 16.

Androulidakis, Y.S., Kourafalou, V.H., 2011. Evolution of a buoyant outflow in the presence of complex topography: the Dardanelles plume (North Aegean Sea). J. Geophys. Res.: Oceans 116 (C4).

Androulidakis, Y.S., Krestenitis, Y.N., Kourafalou, V.H., 2012. Connectivity of north aegean circulation to the Black Sea water budget. Continent. Shelf Res. 48, 8–26.

Balopoulos, E.T., Friligos, N.C., 1993. Water circulation and eutrophication in the northwestern Aegean Sea: Thermaikos gulf. *Journal of Environmental Science & Health* Part A 28 (6), 1311–1329.

Brockmann, C., Doerffer, R., Peters, M., Kerstin, S., Embacher, S., Ruescas, A., 2016. Evolution of the C2RCC neural network for Sentinel 2 and 3 for the retrieval of ocean colour products in normal and extreme optically complex waters. ESASP 740, 54.

Cabral, A., Bonetti, C.H., Garbossa, L.H., Pereira-Filho, J., Besen, K., Fonseca, A.L., 2020. Water masses seasonality and meteorological patterns drive the biogeochemical processes of a subtropical and urbanized watershed-bay-shelf continuum. Sci. Total Environ. 749, 141553.

Clementi, E., Pistoia, J., Delrosso, D., Escudier, R., Drudi, M., Grandi, A., Lyubartsev, V., Ciliberti, S.A., Pinardi, N., Masina, S., Coppini, G., 2019. The Mediterranean analysis and forecasting physical system for the Copernicus Marine Service: description and skill assessment. In: GODAE OceanView Symposium 2019-OceanPredict'19.

Deltares, 2018. Delft3D-FLOW, Simulation of Multi-Dimensional Hydrodynamic Flows and Transport Phenomena, Including Sediments, p. 694. User Manual, version: 3.15, SVN Revision: 57696, August 30, 2018.

Dutkiewicz, S., Follows, M.J., Bragg, J.G., 2009. Modeling the coupling of ocean ecology and biogeochemistry. Global Biogeochem. Cycles 23 (4).

Estournel, C., Zervakis, V., Marsaleix, P., Papadopoulos, A., Auclair, F., Perivoliotis, L., Tragou, E., 2005. Dense water formation and cascading in the Gulf of Thermaikos (North Aegean), from observations and modelling. Continent. Shelf Res. 25 (19–20), 2366–2386.

Ferrante, M., Conti, G.O., Fiore, M., Rapisarda, V., Ledda, C., 2013. Harmful algal blooms in the Mediterranean Sea: effects on human health. EuroMediterranean Biomedical Journal 8.

Genitsaris, S., Stefanidou, N., Sommer, U., Moustaka-Gouni, M., 2019. Phytoplankton blooms, red tides and mucilaginous aggregates in the urban Thessaloniki Bay, Eastern Mediterranean. Diversity 11 (8), 136.

Gerritsen, H., De Goede, E.D., Platzek, F.W., Genseberger, M., van Kester, J.A.T.M., Uittenbogaard, R.E., 2007. Validation Document Delft3D-FLOW; a software system for 3D flow simulations. The Netherlands: Delft Hydraulics, Report X 356, M3470.

Gotsis Skretas, O., Friligos, N., 1990. Contribution to eutrophication and phytoplankton ecology in the Thermaikos Gulf. Thalassografika 13, 1–12.

Hillebrand, H., Dürselen, C.D., Kirschtel, D., Pollingher, U., Zohary, T., 1999. Biovolume calculation for pelagic and benthic microalgae. J. Phycol. 35 (2), 403–424.

Hyder, P., Simpson, J.H., Christopoulos, S., Krestenitis, Y., 2002. The seasonal cycles of stratification and circulation in the Thermaikos gulf region of freshwater influence (ROFI), north-west aegean. Continent. Shelf Res. 22 (17), 2573–2597.

Karageorgis, A., Anagnostou, Ch, Georgopoulos, D., Albuisson, M., 2000. Distribution of suspended particulate matter determined by in-situ observations and satellite images in the NW Aegean Sea (Greece). Geo Mar. Lett. 20 (2), 93–100.

Karageorgis, A.P., Skourtos, M.S., Kapsimalis, V., Kontogianni, A.D., Skoulikidis, N.T., Pagou, K., Nikolaidis, N.P., Drakopoulou, P., Zanou, B., Karamanos, H., Levkov, Z., 2005. An integrated approach to watershed management within the DPSIR framework: Axios River catchment and Thermaikos Gulf. Reg. Environ. Change 5 (2–3), 138–160.

Kendall, M., 1975. Multivariate Analysis. Charles Griffin & Company Ltd, London, UK.

Kourafalou, V.H., Barbopoulos, K., 2003. High resolution simulations on the North Aegean Sea seasonal circulation. *Annales Geophysicae,* European Geosciences Union 21 (1), 251–265, 2003.

Kourafalou, V., Tsiaras, K., 2007. A nested circulation model for the North Aegean Sea. *Ocean Science,* European Geosciences Union 3 (1), 1–16.

Krestenitis, Y., Kombiadou, K., Androulidakis, Y., Makris, C., Baltikas, V., Skoulikaris, C., Kontos, Y., Kalantzi, G., 2015. Operational oceanographic platform in Thermaikos gulf (Greece): forecasting and emergency alert system for public use. In: *Proceedings Of 36th International Association Of Hydraulic Research (IAHR) World Congress,* the Hague, The Netherlands, 28 June – 3 July, 2015.

Krestenitis, Y.N., Androulidakis, Y., Kombiadou, K., Makris, C., Baltikas, V., Kalantzi, G., 2014. Operational oceanographic forecasts in the Thermaikos gulf: the WaveForUs project. In: *Proceedings 12th International Conference On Protection and Restoration Of the Environment (PRE),* Skiathos Island, Greece, 29 June – 3 July 2014, ISBN 978-960-88490-6-8, pp. 313–318.

Krestenitis, Y.N., Kolovoyiannis, V., Androulidakis, Y., Makris, C., Baltikas, V., 2020. Circulation patterns and eutrophication phenomena in the Thermaikos Gulf. In: Proceedings of the EGU General Assembly 2020, Vienna, Austria, 3–8 May 2020. https://doi.org/10.5194/egusphere-egu2020-11775.

Krestenitis, Y.N., Kombiadou, K.D., Androulidakis, Y.S., 2012. Interannual variability of the physical characteristics of north Thermaikos gulf (NW Aegean Sea). J. Mar. Syst. 96, 132–151.

Kuhn, A.M., Dutkiewicz, S., Jahn, O., Clayton, S., Rynearson, T.A., Mazloff, M.R., Barton, A.D., 2019. Temporal and spatial scales of correlation in marine phytoplankton communities. J. Geophys. Res.: Oceans 124 (12), 9417–9438.

Lee, J.H., Harrison, P.J., Kuang, C., Yin, K., 2006. Eutrophication dynamics in Hong Kong coastal waters: physical and biological interactions. In: The Environment in Asia Pacific Harbours. Springer, Dordrecht, pp. 187–206.

Lesser, G.R., Roelvink, J.V., Van Kester, J.A.T.M., Stelling, G.S., 2004. Development and validation of a three-dimensional morphological model. Coast Eng. 51 (8–9), 883–915.

Lévy, M., Franks, P.J., Smith, K.S., 2018. The role of submesoscale currents in structuring marine ecosystems. Nat. Commun. 9 (1), 1–16.

Mann, H.B., 1945. Nonparametric tests against trend. Econometrica. Journal of the Econometric Society 245–259.

Mattas, C., Voudouris, K.S., Panagopoulos, A., 2014. Integrated groundwater Resources management using the dpsir approach in a gis environment: a case study from the Gallikos river basin, north Greece. Water 6, 1043–1068. https://doi.org/10.3390/w604104.

Morel, A., Gentili, B., Claustre, H., Babin, M., Bricaud, A., Ras, J., Tieche, F., 2007. Optical properties of the "clearest" natural waters. Limnol. Oceanogr. 52 (1), 217–229.

Moritz, C., Meynard, C.N., Devictor, V., Guizien, K., Labrune, C., Guarini, J.M., 2013. Disentangling the role of connectivity, environmental filtering, and spatial structure on metacommunity dynamics. Oikos 122, 1401–1410.

Nikolaidis, N.P., Karageorgis, A.P., Kapsimalis, V., Marconis, G., Drakopoulou, P., Kontoyiannis, H., Krasakopoulou, E., Pavlidou, A., Pagou, K., 2006. Circulation and nutrient modeling of Thermaikos gulf, Greece. J. Mar. Syst. 60 (1–2), 51–62.

Nikolaidis, G., Koukaras, K., Aligizaki, K., Heracleous, A., Kalopesa, E., Moschandreou, K., Tsolaki, E., Mantoudis, A., 2005. Harmful microalgal episodes in Greek coastal waters. Journal of Biological Research. *Scientific Annals of the School of Biology* 3, 77–85.

Pagou, K., Assimakopoulou, G., Krasakopoulou, E., Pavlidou, A., 2000. Nutrient input, fluxes and cycling in relation to the biological production in Mediterranean ecosystems influenced by river discharges: Thermaikos Gulf (Greece). In: Dynamics of Matter Transfer and Biogeochemical Cycles: Their Modelling in Coastal Systems of the Mediterranean Sea: Final Scientific Report. 1, pp. 50–81, 2000.

Petala, M., Tsiridis, V., Androulidakis, I., Makris, C., Baltikas, V., Stefanidou, A., Genitsaris, S., Antoniadou, C., Rammou, D., Moustaka-Gouni, M., Chintiroglou, C.C., Darakas, E., 2018. Monitoring the marine environment of Thermaikos gulf. In: *Proc. Of PRE-XIV Conference*, in Chapter: Protection and Restoration of Ecosystems, Thessaloniki, Greece, 3-6 July 2018, ISBN 978-960-99922-4-4, pp. 762–774.

Pinardi, N., Arneri, E., Crise, A., Ravaioli, M., Zavatarelli, M., 2006. The physical, sedimentary and ecological structure and variability of shelf areas in the Mediterranean sea (27). Sea 14, 1243–1330.

Poulos, S.E., Chronis, G.Th, Collins, M.B., Lykousis, V., 2000. Thermaikos Gulf Coastal System, NW Aegean Sea: an overview of waterrsediment fluxes in relation to air–land–ocean interactions and human activities. J. Mar. Syst. 25, 47–76, 2000.

Pytharoulis, I., Tegoulias, I., Kotsopoulos, S., Bampzelis, D., Kartsios, S., Zanis, P., Katragkou, E., Karacostas, T., 2014. High-resolution WRF hindcasts over central Greece: characteristics of simulated convective activity and model evaluation. In: Proceedings of the 15th Annual WRF Users' Workshop, Boulder, Colorado, USA, vol. 25.

Rabalais, N.N., Turner, R.E., Díaz, R.J., Justić, D., 2009. Global change and eutrophication of coastal waters. ICES (Int. Counc. Explor. Sea) J. Mar. Sci. 66 (7), 1528–1537.

Sea-Bird Scientific, 2017. Seasoft V2: SBE data processing CTD data processing & plotting software for windows. Software Manual.

Simoncelli, S., Fratianni, C., Pinardi, N., Grandi, A., Drudi, M., Oddo, P., Dobricic, S., 2019. Mediterranean Sea Physical Reanalysis (CMEMS MED-Physics). https://doi.org/10.25423/MEDSEA_REANALYSIS_PHYS_006_004. Copernicus Monitoring Environmen, t Marine Service (CMEMS). [Data set].

Skogen, M.D., Eilola, K., Hansen, J.L., Meier, H.M., Molchanov, M.S., Ryabchenko, V.A., 2014. Eutrophication status of The north sea, skagerrak, kattegat and the baltic sea in present and future climates: a model study. J. Mar. Syst. 132, 174–184.

Skoulikaris, C., Krestenitis, Y., 2020. Cloud data scraping for the assessment of outflows from dammed rivers in the EU. A case study in south eastern europe. Sustainability 12 (19), 7926.

Skoulikidis, N.T., 1993. Significance evaluation of factors controlling river water composition. Environ. Geol. 22 (2), 178–185.

Smardon, R., 2009. *The Axios River Delta – Mediterranean Wetland under Siege.* Sustaining the World's Wetlands. Springer, New York, pp. 57–92.

Sommer, U., Charalampous, E., Scotti, M., Moustaka-Gouni, M., 2018. Big fish eat small fish: implications for food chain length? Community Ecol. 19 (2), 107–115.

Sur, H.İ., Özsoy, E., Ünlüata, Ü., 1994. Boundary current instabilities, upwelling, shelf mixing and eutrophication processes in the Black Sea. Prog. Oceanogr. 33 (4), 249–302.

Tsiaras, K.P., Petihakis, G., Kourafalou, V.H., Triantafyllou, G., 2014. Impact of the river nutrient load variability on the North Aegean ecosystem functioning over the last decades. J. Sea Res. 86, 97–109.

Utermöhl, H., 1958. Zur vervollkommnung der quantitativen phytoplankton-methodik: mit 1 Tabelle und 15 abbildungen im Text und auf 1 Tafel. Internationale Vereinigung für theoretische und angewandte Limnologie: Mitteilungen 9 (1), 1–38.

Veranis, N., Chrysafi, A., Makrovasili, K., 2011. Hydrogeological conditions of the lower reaches of Aliakmonas and Loudias rivers aquifer system, Region of Central Macedonia, Northern Greece. In: Advances in the Research of Aquatic Environment. Springer, Berlin, Heidelberg, pp. 357–364.

Vokou, D., Giannakou, U., Kontaxi, C., Vareltzidou, S., 2018. Axios, aliakmon, and Gallikos delta complex (northern Greece). The Wetland Book 1137–1147. https://doi.org/10.1007/978-94-007-4001-3_253.

Wang, X., Liang, X.Z., Jiang, W., Tao, Z., Wang, J.X., Liu, H., Han, Z., Liu, S., Zhang, Y., Grell, G.A., Peckham, S.E., 2010. WRF-Chem simulation of East Asian air quality: sensitivity to temporal and vertical emissions distributions. Atmos. Environ. 44 (5), 660–669.

Zavatarielli, M., Mellor, G.L., 1995. A numerical study of the Mediterranean Sea circulation. J. Phys. Oceanogr. 25 (6), 1384–1414.

Zervakis, V., Georgopoulos, D., 2002. Hydrology and circulation in The north aegean (eastern mediterranean) throughout 1997 and 1998. Mediterr. Mar. Sci. 3 (1), 5–19.

Zervakis, V., Karageorgis, A.P., Kontoyiannis, H., Papadopoulos, V., Lykousis, V., 2005. Hydrology, circulation and distribution of particulate matter in Thermaikos gulf (NW Aegean Sea), during september 2001–october 2001 and february 2002. Continent. Shelf Res. 25 (19–20), 2332–2349.

Zohdi, E., Abbaspour, M., 2019. Harmful algal blooms (red tide): a review of causes, impacts and approaches to monitoring and prediction. Int. J. Environ. Sci. Technol. 16 (3), 1789–1806.